Volume 12. Number 2. 167-193 NOVEMBER 2023

Jurnal Ilmiah Pendidikan Fisika Al-BiRuNi
https://ejournal.radenintan.ac.id/index.php/al-biruni/index
DOI: 10.24042/jipfalbiruni.v12i2.18008

P-ISSN: 2303-1832
e-ISSN: 2503-023X

Thermodynamic and Magnetic Properties of Diatomic Molecules for Non-central Potentials under the Influence of External Magnetic Fields

Cari[1*], Luthfiya Kurnia Permatahati[2], A Suparmi[1]

[1]Faculties Member of Physics Department, Universitas Sebelas Maret, Indonesia
[2]Doctoral Student of Physics Department, Universitas Sebelas Maret, Indonesia

**Corresponding Address: cari@staff.uns.ac.id*

Article Info

Article history:

Received: July 11, 2023
Accepted: September 24, 2023
Published: November 29, 2023

Keywords:

Thermodynamic properties;
magnetic properties;
Schrodinger equation;
noncentral potential;
magnetic field.

ABSTRACT

This paper studies the thermodynamic and magnetic properties of some diatomic molecules governed by Scarf and Morse non-central potentials under external magnetic and electric fields. The Schrodinger equation with Scarf and Morse non-central potentials is solved using Supersymmetric WKB quantization conditions to obtain the energy equation and wave function. The influence of the magnetic and electric fields on the energy eigenvalue was discussed. The results show that energy increases with the increasing magnetic field and decreases with the increasing electric field. Moreover, the thermodynamic and magnetic properties involving internal energy, free energy, specific heat capacity, entropy, magnetization, magnetic susceptibility, and persistent current were determined by calculating the partition function. The internal energy increases linearly with the increasing magnetic field for a given temperature. Meanwhile, the specific heat capacity decreases with the increasing magnetic field. We point out that the presence of magnetic and electric fields makes the system exhibit diamagnetic behavior.

INTRODUCTION

In recent years, the physical properties of low-dimensional semiconductor nanostructures have attracted much attention from many scientists. The low-dimensional structures are widely applicable to chemistry, physics, and engineering. The low-dimensional structures have a unique structure, characteristics, and sensitivity to external factors such as pressure, temperature, magnetic fields, electric fields, and impurity states, which has opened up a broad branch of interdisciplinary research. For example, in electronics, numerous low-dimensional materials have demonstrated superior performance in photodetectors, field-effect transistors, and some flexible devices (Comtet et al., 1985; Dutt et al., 1988; Fang et al., 2019; Zeiri et al., 2019). In applying photodetectors, the variety of low-dimensional materials and properties enable wide-spectrum detection from ultraviolet to infrared, which provides a potential option for photodetectors under different conditions.

The low-dimensional materials provide unparalleled advantages for flexible electronic devices due to their high performance and mechanical stability. Moreover, low-dimensional materials have good application prospects in optoelectronics because of the change of carrier transport caused by surface defects and size and the good optoelectric properties of the materials themselves. Also, it has to be noted that some low-dimensional materials are sensitive to deformation (Peleshchak et al., 2020), making them

How to cite Cari, C., Permatahati, L. K., & Suparmi, A. (2023). Thermodynamic and magnetic properties of diatomic molecules for non-central potentials under the influence of external magnetic fields. *Jurnal ilmiah pendidikan fisika Al-Biruni, 12*(2), 167-193.

useful as mechanical strain sensors for studying and controlling the characteristics of nanomaterials (Li et al., 2019; Lin et al., 2013; Xiao et al., 2016). There are several techniques to fabricate nanostructures, such as droplet epitaxy, chemical vapor deposition, molecular-beam epitaxy, and lithography (Fuhrmann et al., 2005; Soopy et al., 2021; Wang et al., 2008). The techniques can produce structures of different geometries, including spherical, cylindrical, double-quantum rings, rectangular, and single-quantum rings (Mano et al., 2005).

Statistical physics can be used to study the physical properties of a system because it can interpret and forecast thermodynamic properties in systems made up of numerous particles as well as several phenomena of matter using the statistical average of dynamic amounts over a particular number of particles (Ortega & Hernandez, 2018). Several thermodynamic and magnetic properties involving heat capacity, free energy, entropy, magnetic susceptibility, magnetization, and internal energy reveal some significant properties of a molecule that are highly relevant to applications in photonics, micro-electronics, and biomedicine (Ikot et al., 2019; Jiang et al., 2019; Khosla et al., 2023; Okorie, Ikot, et al., 2020). The reason is that the thermodynamic properties provide insights into the arrangement and how particles are distributed throughout the nanomaterial (Jia et al., 2019; Jia et al., 2017). It is crucial in characterizing the thermal behavior, the energy distribution, the heat transfer mechanisms, and determining their phase transitions, stability, and equilibrium states (Khosla et al., 2023).

Investigating the thermodynamic and magnetic properties of the system is particularly interesting. We must solve the Schrodinger equation that closely approximates the real information on the evolution of the above systems (Jia et al., 2017). The Schrodinger equation has been modeled using various potentials to explain the physical systems. Omar has solved the PDM Schrodinger equation with Yukawa plus Kratzer potential, known as the confinement potential type commonly used in the spectroscopy of diatomic molecules (Omar Mustafa, 2020). Here is the expression of the PDM Schrodinger equation:

$$\left[\frac{\hat{P}(\vec{r})-e\vec{A}(\vec{r})}{\sqrt{m(\vec{r})}}+W(\vec{r})\right]\psi(\vec{r})=$$
$$E\psi(\vec{r});\ W(\vec{r})=e\varphi(\vec{r})+V(\vec{r})$$

Further, the Schrodinger with Eckart potential, which is a diatomic molecular potential model has also been investigated to determine thermodynamic stability (Onate et al., 2018), Faniandari et al. (2023) studied the thermomagnetic properties of diatomic molecule for exponential potential which is suitable to describe how diatomic molecules behave and interact, and other potentials (Dong et al., 2018; Okon et al., 2017) have been applied in the Schrodinger equation and obtained the exact solutions by using different methods such as the hypergeometric method (Dianawati et al., 2019), Nikiforov-Uvarov method (Assi et al., 2018; Hassanabadi, Maghsoodi, et al., 2018), Lie algebraic method (Hassanabadi, Chung, et al., 2018), Asymptotic Iteration Method (AIM) (Faniandari et al., 2023), and Supersymmetric Quantum Mechanics method (Suparmi et al., 2020). In a diatomic molecule, the Morse potential provides an excellent qualitative representation of the interaction between two atoms (Morse, 1929). This potential is one of the most successful and convenient models for explaining diatomic molecules' rotational and vibrational structure (Rosen & Morse, 1932). Another potential that plays an essential role in different disciplines of physics, from electrodynamics to particle theory, is the Scarf potential. Scarf potential admits beautiful formulations for discrete eigenvalues (Dabrowaska et al., 1988; Gendenshtien, 1983; Houtot, 1973). This potential has contributed immensely to

supersymmetric quantum mechanics, group theory, and quantum mechanical studies. More accurate periodic potential in crystals can be created with the Scarf potential than the trigonometric Scarf one (Levai, 1994). Scarf is discussed as a problem of non-central potentials in electrodynamics (Li & Kusnezov, 1999). In particles, Scarf appears in the application of the nonperturbative sector of gauge theories (Li & Kusnezov, 1999).

Supersymmetric quantum mechanics (SUSY-QM) is one of the most recent and powerful methods of solving the Schrodinger equation (Castillo & Kirchbach, 2007). SUSYQM was initially proposed as a model for understanding SUSY breaking in nature. However, it started to walk alone as a helpful tool in nonrelativistic quantum mechanics. Based on the supersymmetry field, SUSYQM theory provides a direct method for the precise solution of the Schrodinger equation. It allows one to calculate the eigenvalues and eigenfunctions analytically using the algebraic operator formulation for the solvable potentials model without solving the Schrodinger-like differential equation via the standard series method. The key is to identify the superpotential of the solvable potential and then calculate the corresponding shape invariance.

The energy eigenvalues can be obtained according to the superpotential, and the wave functions can be obtained by lowering and raising SUSY operators (Suparmi & Cari, 2014). Therefore, it is very simple to solve the Schrodinger equation using SUSYQM. Inspired by the semiclassical WKB quantization condition, the modified semiclassical WKB quantization condition was constructed for SUSY Hamiltonian *H-* (Comtet et al., 1985). Surprisingly, the modified semiclassical WKB quantization condition provides exact bound state energy spectra for a class of shape-invariant potentials, which is compared to the WKB quantization condition that has to be supplemented by Langer-like correction (Comtet et al., 1985; Gangopadhyaya et al., 2021). The modified semiclassical quantization condition is then named the SWKB quantization condition. It has been discovered to provide better accuracy results than the WKB quantization condition for many problems and be exact for all shape-invariant potentials. For shape-invariant potentials, the SWKB quantization condition is exact not only for the ground state (exact by construction) and for large n (as any correct semiclassical result should be) but also for all intermediates n (Yin et al., 2010).

Many authors have used SUSY-QM to investigate the Schrodinger equation with various potentials. Suparmi et al. (Suparmi et al., 2020) used SUSYQM to obtain the solution of the Schrodinger equation for modified Woods–Saxon and Eckart potentials in toroidal coordinates. Abu-Shady and Ikot applied the SUSYQM method to solve the multi-dimensional Schrodinger equation with the heavy-quarkonia potential (Abu-Shady & Ikot, 2019). The Schrodinger equation for the Manning-Rosen plus Hulthen potential has been solved by Ahmadov et al. using SUSYQM to obtain the energy levels (Ahmadov et al., 2018). Considering the above reasons, in this work, we use the analytical approximation of the SWKB quantization condition to solve the Schrodinger equation with Scarf and Morse non-central potentials. The energy eigenvalue is determined analytically using the approximation of the SWKB quantization condition, but exceptionally, it yields the exact result. The wave function is determined using the SUSY operator. The bound state energy equation is applied to obtain the partition function used to analyze diatomic molecules' thermodynamic and magnetic properties.

The thermodynamic and magnetic properties are closely related to the study of magnetocaloric properties, defined as the variation of temperature of a material in reaction to a changing magnetic field

(Biswas et al., 2019; Castro et al., 2020). This effect was found by Warburg in 1881 by applying a magnetic field to the Fe molecule (Warburg, 1881). The magnetocaloric properties attract the attention of researchers since they are defined as the intrinsic property of magnetic materials under the influence of a magnetic field, which is expressed by a change in temperature (Zhang et al., 2016; Zhang, 2016). Gschneidner, Pecharsky, and Tsokol (Gschneidner et al., 2005) studied the effect of magnetocaloric and described the reversible change in temperature of material under adiabatic conditions produced by the magnetic entropy change due to the variation in an applied magnetic field.

Nowadays, the study of thermodynamic and magnetic properties is broadened to the system influenced by an external magnetic field. Edet (Edet et al., 2022) has studied the magnetic properties of LiH diatomic molecules in the system under the influence of the magnetic and Aharonov-Bohm fields. The presence of external fields has significantly impacted quantum mechanics since it affects the behavior of the energy spectra of a system (Edet & Ikot, 2021), typically by creating shifts or removing degeneracy. In the other work, Rastegar Sedehi and Khordad (Sedehi & Khordad, 2021) investigated the magnetic properties of tuned quantum dot/ring systems. Regarding the previous work, the Schrodinger equation with several diatomic molecular potential models has been investigated by many authors to study the energy levels of particles (involving a diatomic molecule) and their thermodynamic functions. They employed the hypergeometric method, the NU method, and AIM to solve the Schrodinger equation analytically. In the current work, the Schrodinger equation under external magnetic and electric fields with the Scarf and Morse non-central potentials will be solved using the SUSY method to obtain the energy levels, followed by determining the thermodynamic and magnetic properties of H_2, LiH, and HCl diatomic molecules. These three different diatomic molecules were chosen because they are currently widely researched regarding the various benefits they have, including research on H_2 as a new energy source (Pareek et al., 2020), LiH as an H_2 storage material and conductor Li+ ions (Banger et al., 2018), and HF, which is very useful in chemical and biological applications since it is a stable species in certain conditions (Orabi & Faraldo-Gómez, 2020).

Based on the above points, this paper aims to analyze the thermodynamic and magnetic properties of the combined system of the Scarf and Morse non-central potentials under external magnetic and electric fields. The energy spectra and the thermodynamic and magnetic properties of H_2, LiH, and HCl diatomic molecules were investigated. In section 1, we present the introduction; in section 2, we discuss the Scarf and Morse non-central effective potentials; and in the third section, the basic theory of SUSY-QM is discussed. The Schrodinger equation with the Scarf and Morse non-central potentials in the presence of external magnetic and electric fields is solved using the SWKB quantization condition, followed by an analysis of the thermodynamic and magnetic properties of the system discussed in the fourth section. The last section is the conclusion.

THEORY AND METHODS

We consider an electron confined in the Scarf and Morse non-central potentials under magnetic field perturbation. The Hamiltonian of the system is given by (Bala et al., 2017; Solaimani, 2021; Vicente et al., 2021):

$$H = \frac{(P+eA)^2}{2M} + V(r,\theta,z) - eFr \quad (1)$$

Where M is the effective mass of the electron, in cylindrical coordinates, θ is the angle between the z axes and $\vec{r}$ vector, shown in Figure 1, $r\sin\theta = \rho, r\cos\theta = z$, and ρ is the radius of the cylinder cross-section. F is the electric field in the z-direction, and the magnetic field's vector

potential, $\vec{A} = \left(\frac{B\rho}{2}\right)\hat{\varphi}_0$, is taken in the symmetric gauge. The V in equation (1) is the confinement potential, which is expressed as (Nikiforov & Uvarov, 1988):

$$V(r,\theta,z) = V_{c1}(r,\theta) + V_{c2}(z) \quad (2)$$

Where:

$$V_{c1} = \frac{\hbar^2}{2M}\left(\frac{C}{r^2 sin^2 2\theta} + \frac{Dcos2\theta}{r^2 sin^2 2\theta}\right) = \frac{\hbar^2}{2M}\left(\frac{C+D}{4\rho^2} + \frac{C-D}{4z^2}\right) \quad (3)$$

And V_{c2} is Morse potential in z-direction given as:

$$V_{c2}(z) = \frac{\hbar^2}{2M}\left(-2D_e e^{-\alpha(z-z_0)} + D_e e^{-2\alpha(z-z_0)}\right) \quad (4)$$

Where D_e is the dissociation energy, the parameter α represents the potential width, z_0 is the equilibrium internuclear distance, and *C* and *D* are two potential parameters.

The Schrodinger equation that is influenced by a uniform magnetic field and electric field in the z-direction given in equation (1) with confinement potential $V = V_{c1}(\rho,z) + V_{c2}(z)$ given in equations (2) is rewritten as:

$$\left\{\left(p^2 + \frac{e}{c}\overline{p}.\bar{A} + \frac{e}{c}\bar{A}.\overline{p} + \left(\frac{e}{c}\bar{A}\right)^2\right) + 2M(V_{c1}(\rho,z) + V_{c2}(z) - E - eFz)\right\}\Psi(\rho,\varphi,z) = 0 \quad (5)$$

With:

$$p^2 = -\hbar^2\Delta;\ \ \Delta = \frac{1}{\rho}\frac{d}{d\rho}\left(\rho\frac{d}{d\rho}\right) + \frac{1}{\rho^2}\frac{d^2}{d\varphi^2} + \frac{d^2}{dz^2};\quad \nabla = \hat{\rho}_0\frac{d}{d\rho} + \frac{\hat{\varphi}_0}{\rho}\frac{d}{d\varphi} + \hat{z}_0\frac{d}{dz} \quad (6)$$

By using equations (3)-(6) the Schrodinger equation in equation (5) becomes:

$$\left\{\left(-\hbar^2\left(\frac{1}{\rho}\frac{d}{d\rho}\left(\rho\frac{d}{d\rho}\right) + \frac{1}{\rho^2}\frac{d^2}{d\varphi^2} + \frac{d^2}{dz^2}\right) - 2i\frac{e\hbar}{c}\left(\left(\frac{B\rho}{2}\right)\right)\frac{1}{\rho}\frac{d}{d\varphi} + \left(\frac{e}{c}\left(\frac{B\rho}{2}\right)\right)^2\right) + 2M\left(\frac{\hbar^2}{2M}\left(-2D_e e^{-\alpha(z-z_0)} + D_e e^{-2\alpha(z-z_0)}\right) + \frac{\hbar^2}{2M}\left(\frac{C+D}{4\rho^2} + \frac{C-D}{4z^2}\right) - E - eFz\right)\right\} g(\rho)\chi(z)e^{im\varphi} = 0 \quad (7)$$

By substituting the wave function $\Psi(\rho,\varphi,z) = g(\rho)\chi(z)e^{im\varphi}$, the Schrodinger equation can be resolved (Okon et al., 2022), where $m = 0, \pm1, \pm2, \ldots, \pm l$ is the magnetic quantum number, and l is the angular momentum quantum number.

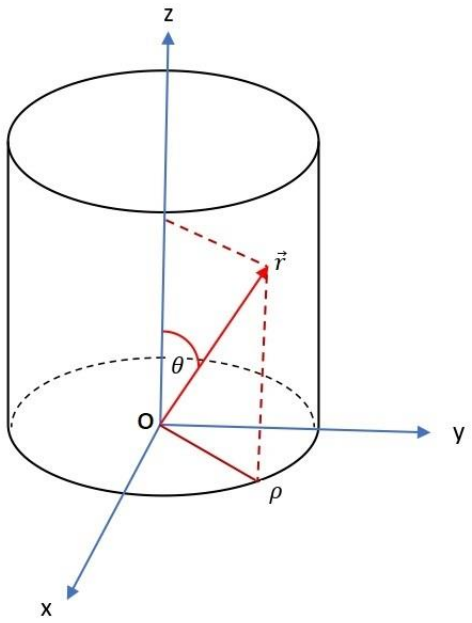

Figure 1. Cylindrical Coordinate

The radial equation can also be further simplified to $g(\rho) = \frac{f_{mn}}{\sqrt{\rho}}$. Then equation (7) is simplified as:

$$\left\{\left(-\hbar^2\left(\chi(z)e^{im\varphi}\frac{1}{\rho}\frac{d}{d\rho}\left(\rho\frac{d\frac{f_{mn}}{\sqrt{\rho}}}{d\rho}\right) + \frac{f_{mn}}{\sqrt{\rho}}\chi(z)\frac{1}{\rho^2}\frac{d^2e^{im\varphi}}{d\varphi^2} + \frac{f_{mn}}{\sqrt{\rho}}e^{im\varphi}\frac{d^2\chi(z)}{dz^2}\right) -\right.\right.$$

$$2i\frac{e\hbar}{c}\frac{f_{mn}}{\sqrt{\rho}}\chi(z)\left(\left(\frac{B\rho}{2}\right)\right)\frac{1}{\rho}\frac{de^{im\varphi}}{d\varphi}\Bigg)+\left[\left(\frac{e}{c}\left(\frac{B\rho}{2}\right)\right)^2+2M(V_{c1}(\rho,z)+V_{c2}(z)-E-eFz)\right]\frac{f_{mn}}{\sqrt{\rho}}\chi(z)e^{im\varphi}\Bigg\}=0 \quad (8)$$

At this point, the eigenvalue and eigenfunction in equation (8) will have their "spectral signatures" on the overall spectra within the three-dimensional cylindrical settings (Okon & al., 2022). So we are interested only in the radial part and z part of the Schrodinger equation, which can result from equation (8) as follows:

$$-\frac{1}{f_{mn}}\left(f''_{mn}+\left(\frac{1}{4}-m^2\right)\frac{f_{mn}}{\rho^2}\right)+2\frac{me}{\hbar c}\left(\left(\frac{B\rho}{2}\right)\right)\frac{1}{\rho}+\left[\frac{1}{\hbar^2}\left(\frac{e}{c}\left(\frac{B\rho}{2}\right)\right)^2+\frac{2M}{\hbar^2}\left(V_{c1}(\rho)-E_\rho\right)\right]=0 \quad (9)$$

$$\frac{1}{\chi(z)}\frac{d^2\chi(z)}{dz^2}-\frac{2M}{\hbar^2}(V_{c1}(z)+V_{c2}(z)-E_z-eFz)=0 \quad (10)$$

The radial Schrodinger equation in equation (9) can be simplified mathematically into:

$$f''_{mn}-\left[\frac{e^2B^2}{4\hbar^2c^2}\rho^2+\frac{2M}{\hbar^2}\left(\frac{C+D-\left(1-4m^2\right)\hbar^2/2M}{4\rho^2}\right)\right]f_{mn}+\left(\frac{2M}{\hbar^2}E_\rho-\frac{meB}{2\hbar c}\right)f_{mn}=0 \quad (11)$$

with the radial effective potential given as:

$$V_{eff}(\rho)=\left\{\frac{C+D}{4}-\frac{\hbar^2}{2M}\left(\frac{1}{4}-m^2\right)\right\}\frac{1}{\rho^2}+\frac{e^2}{2\mathrm{M}c^2}\frac{B^2\rho^2}{4} \quad (12)$$

And:

$$E'_\rho=E_\rho-\frac{meB}{2\hbar c}\frac{\hbar^2}{2M} \quad (13)$$

Meanwhile, the z part of the Schrodinger equation obtained from equation (10) is rewritten as:

$$\frac{d^2\chi(z)}{dz^2}-\frac{2M}{\hbar^2}\left(\frac{C-D}{4z^2}-2D_e e^{-\alpha_z(z-z_0)}+D_e e^{-2\alpha_z(z-z_0)}-eFz\right)\chi(z)+\frac{2ME_z}{\hbar^2}\chi(z)=0 \quad (14)$$

with the effective potentials in the z-direction given as:

$$V_{eff}(z)=\frac{C-D}{4z^2}-2D_e e^{-\alpha_z(z-z_0)}+D_e e^{-2\alpha_z(z-z_0)}-eFz \quad (15)$$

The Scarf and Morse potentials with $z=0$ are not exactly solvable; consequently, our numerical results can't be checked against the exact ones. Despite that, some recent numerical and perturbative works have been reported (Ikhdair & Falaye, 2013; Ikhdair & Hamzani, 2012). The most widely used approximation, which is based on the expansion of the centrifugal term $l(l+1)z^{-2}$ in a series of exponential terms around the equilibrium inter-nuclear position $z=z_0(\rho=0)$ of the Morse oscillator potential by keeping terms up to second order $z=z_0$ (i. e. at low excitation energy, where $z\approx z_0$), it was proposed by (Pekeris, 1934). The Pekeris approximation is truncated at the quartic term and is primarily based on expanding powers of exponential functions. The following exponential form can be used instead of the centrifugal term:

$$\frac{1}{z^2}=D_0+D_1e^{-\beta\prime x}+D_2e^{-2\beta\prime x} \quad (16)$$

Which can be expanded around the minimum point $z\approx z_0$or $(x=0)$ only up to the second order as:

$$\frac{1}{z^2}=D_0+D_1+D_2-\frac{\beta'}{4}(D_1+D_2)x+\frac{\beta'^2}{16}D_2x^2-\cdots \quad (17)$$

It only approximates the lower-excitation rotation energy states well, but since there are large inter-atomic separations, it will be hard to describe the higher-excitation rotation energy states (Okorie & Ibekwe, 2018). The expression of centrifugal term $\frac{1}{z^2}$ can also be expanded around $x = 0$ up to the second-order term (Ikhdair & Falaye, 2013):

$$\frac{1}{z^2} = \frac{1}{z_0^2}(1 - 2x + 3x^2 - \cdots) \quad (18)$$

Comparing equations (17) and (18), the constant parameters for the Scarf and Morse potentials determined by:

$$D_0 = 1 - \frac{3}{\alpha_z z_0} + \frac{3}{\alpha_z^3 z_0^2} = 1 - \frac{3}{\beta\prime} + \frac{3}{\beta\prime^2} \quad (19a)$$

$$D_1 = \frac{4}{\alpha_z z_0} - \frac{6}{\alpha_z^3 z_0^2} = \frac{4}{\beta\prime} - \frac{6}{\beta\prime^2} \quad (19b)$$

$$D_2 = -\frac{1}{\alpha_z z_0} + \frac{3}{\alpha_z^3 z_0^2} = -\frac{1}{\beta\prime} + \frac{3}{\beta\prime^2} \quad (19c)$$

With:

$$x = \frac{(z-z_0)}{z_0}, \quad \beta' = \alpha_z z_0, \qquad z = \frac{1}{\alpha_z} + z_0 - \frac{e^{-\alpha_z(z-z_0)}}{\alpha_z} \quad (20)$$

The Schrodinger equation in z-direction obtained from equations (15)-(20), such that:

$$\frac{d^2\chi(z)}{dz^2} - \frac{2M}{\hbar^2}\left(-\left(2D_e - \frac{(C-D)D_1}{4} + \frac{eF}{\alpha_z}\right)e^{-\alpha_z(z_z-z_0)} + \left(D_e + \frac{(C-D)D_2}{4}\right)e^{-2\alpha_z(z-z_0)}\right)\chi(z) + \frac{2M}{\hbar^2}\left(E_z - \frac{(C-D)D_0}{4} + \frac{eF}{\alpha_z} + eFz_0\right)\chi(z) = 0 \quad (21)$$

To simplify equation (21), we have defined the dimensionless parameters as follows:

$$T = -\left(2D_e - \frac{(C-D)D_1}{4} - \frac{eF}{\alpha_z}\right)e^{\alpha_z(z_0)}, \quad A = \left(D_e + \frac{(C-D)D_2}{4}\right)e^{2\alpha_z(z_0)} \quad (22)$$

$$E_z' = E_z - \frac{(C-D)D_0}{4} + \frac{eF}{\alpha_z} + eFz_0 \quad (23)$$

Then, the effective Morse-like potential in equation (15) reduces as:

$$V(z) = Ae^{-2\alpha_z z} + Te^{-\alpha_z z} \quad (24)$$

The energy eigenvalue in ρ and z directions are determined using the SWKB quantization condition, and the associated wave functions are obtained using SUSY operators.

1. Supersymmetry Quantum Mechanics (SUSY-QM)

In 1981, Witten proposed Supersymmetric Quantum Mechanics (SUSY-QM) as a model of one-dimensional field theory in his pioneering work (Witten, 1981) to comprehend how Supersymmetry has been broken in nature. SUSY was anticipated to be broken in nature since no evidence has been reported so far for the existence of particles predicted by supersymmetric schemes. If SUSY was physically meaningful, the symmetry was broken. The key players in SUSY-QM are supercharged operators, which the SUSY Hamiltonian may express. Even though SUSY-QM was initially developed as a model for comprehending SUSY breaking, it has since begun to stand independently, irrespective of its original purpose, as a helpful tool of nonrelativistic quantum mechanics.

The application of SUSY to nonrelativistic quantum mechanics has resulted in a better understanding of exactly solvable potential (Dutt et al., 1988; Sukumar, 1985), simplifying the resolution of the system of Ricatti equation, modified WKB approximation, and so on. In particular, inspired by the semiclassical WKB quantization condition formula, a modified semiclassical WKB quantization condition that was constructed by using SUSY Hamiltonian $H_{\_}$ was proposed by Comtet, Bandrouk, and Campbell (CBC)

has brought an impact on the study of quantum mechanics. The SWKB (CBC) quantization condition formula provides exact bound state energy spectra for the class of shape-invariant potentials; this contrasts with standard WKB quantization, which a Langer-like ad hoc correction must supplement to get the same spectra. A supersymmetry quantum system, as defined by Witten, has supercharge operators $Q_{i,}$ which commute with the Hamiltonian H_{ss} (Witten, 1981) and is denoted as:

$$[Q_i, H_{SS}] = 0 \text{ with, } i = 1, 2, 3, \dots, N \qquad (25)$$

And they obey to anti commutation algebra:

$$\{Q_{i,} Q_j\} = \delta_{ij} H_{ss} \qquad (26)$$

with H_{ss} is referred to supersymmetric Hamiltonian. According to Witten, the simplest SUSY-QM system has N=2, where the supercharge operators are expressed as:

$$Q_1 = \frac{1}{\sqrt{2}}\left(\sigma_1 \frac{p}{\sqrt{2m}} + \sigma_2 \phi(x)\right) \text{ and } Q_2 = \frac{1}{\sqrt{2}}\left(\sigma_2 \frac{p}{\sqrt{2m}} - \sigma_1 \phi(x)\right) \qquad (27)$$

Where σ_i is the usual Pauli spin matrices, $p = -i\hbar \frac{d}{dx}$ is the usual momentum operator, and $\phi(x)$ is superpotential. By applying Pauli matrices, which are given as:

$$\sigma_x = \sigma_1 = \begin{pmatrix} 0 & 1 \\ 1 & 0 \end{pmatrix}, \sigma_y = \sigma_2 = \begin{pmatrix} 0 & -i \\ i & 0 \end{pmatrix} \qquad (28)$$

Then, from equations (27)-(28), we have:

$$Q_1 = \frac{1}{\sqrt{2}} \begin{pmatrix} 0 & \frac{p}{\sqrt{2m}} - i\phi(x) \\ \frac{p}{\sqrt{2m}} + i\phi(x) & 0 \end{pmatrix} \qquad (29)$$

$$Q_1^2 = \frac{1}{\sqrt{2}} \begin{pmatrix} \left\{ \begin{matrix} \left(\frac{p}{\sqrt{2m}}\right)^2 + \\ \left(i\frac{p}{\sqrt{2m}}\phi(x)\right) \\ +\phi^2(x) \end{matrix} \right\} & 0 \\ 0 & \left\{ \begin{matrix} \left(\frac{p}{\sqrt{2m}}\right)^2 - \\ \left(i\frac{p}{\sqrt{2m}}\phi(x)\right) \\ +\phi^2(x) \end{matrix} \right\} \end{pmatrix} \qquad (30)$$

and

$$Q_2 = \frac{1}{\sqrt{2}} \begin{pmatrix} 0 & -i\frac{p}{\sqrt{2m}} - \phi(x) \\ i\frac{p}{\sqrt{2m}} - i\phi(x) & 0 \end{pmatrix} \qquad (31)$$

$$Q_2^2 = \frac{1}{2} \begin{pmatrix} \left\{ \begin{matrix} \left(\frac{p}{\sqrt{2m}}\right)^2 + \\ \left(i\frac{p}{\sqrt{2m}}\phi(x)\right) \\ +\phi^2(x) \end{matrix} \right\} & 0 \\ 0 & \left\{ \begin{matrix} \left(\frac{p}{\sqrt{2m}}\right)^2 - \\ \left(i\frac{p}{\sqrt{2m}}\phi(x)\right) \\ +\phi^2(x) \end{matrix} \right\} \end{pmatrix} \qquad (32)$$

From equations (30) and (32), we obtain the SUSY Hamiltonian given as:

$$H_{ss} = 2Q_1^2 = 2Q_2^2 = \begin{pmatrix} \left\{ \begin{matrix} -\frac{\hbar^2}{2m}\frac{d^2}{dx^2} + \\ \frac{\hbar}{\sqrt{2m}}\frac{d\phi(x)}{dx} + \phi^2(x) \end{matrix} \right\} & 0 \\ 0 & \left\{ \begin{matrix} -\frac{\hbar^2}{2m}\frac{d^2}{dx^2} - \\ \frac{\hbar}{\sqrt{2m}}\frac{d\phi(x)}{dx} + \phi^2(x) \end{matrix} \right\} \end{pmatrix} \qquad (33)$$

$$H_{ss} = \begin{pmatrix} H_+ & 0 \\ 0 & H_- \end{pmatrix}$$

With:

$$H_- = -\frac{\hbar^2}{2m}\frac{d^2}{dx^2} + V_-(x) \quad \text{for} \quad V_-(x) = \phi^2(x) - \frac{\hbar}{\sqrt{2m}}\phi'(x) \qquad (34)$$

And:

$$H_+ = -\frac{\hbar^2}{2m}\frac{d^2}{dx^2} + V_+(x) \quad \text{for} \quad V_+(x) = \phi^2(x) + \frac{\hbar}{\sqrt{2m}}\phi'(x) \tag{35}$$

Here, H_- and H_+ are supersymmetry partners of the Hamiltonian, and $V_-(x)$ and $V_+(x)$ are the supersymmetry partner potential. The new operators are presented as follows to ease the determination of the wave functions:

$$A^+ = -\frac{\hbar}{\sqrt{2m}}\frac{d}{dx} + \phi(x) \quad \text{and} \quad A = \frac{\hbar}{\sqrt{2m}}\frac{d}{dx} + \phi(x) \tag{36}$$

A^+ is the raising operator, and A is the lowering operator. By simple mathematical manipulation from equations (34)-(36), we get:

$$H_- = A^+A, \text{ and } H_+ = AA^+ \tag{37}$$

For a system with good symmetry, the lowering operator annihilates the ground state wave function therefore (Gangopadhyaya et al., 2021):

$$A\psi_0^{(-)} = 0 \tag{38}$$

Subsequently, the excited wave function, $\psi_1^-(x;a_0)$, $\psi_2^-(x;a_0)$, …, $\left(\psi_n^-(x;a_0)\right)$ of H_- are obtained by using a raising operator operated to the lower wave function, given as:

$$\psi_n^-(x;a_0) \approx A^+(x;a_0)A^+(x;a_1)\ldots A^+(x;a_{n-1})\psi_0^{(-)}(x;a_n) \tag{39}$$

which is a generalization of the operator method for the one-dimensional harmonic oscillator potential. The wave function can be obtained from equations (36) and (37). It is always possible to factorize the usual Hamiltonian as:

$$H = H_- + E_0 = -\frac{\hbar^2}{2m}\frac{d^2}{dx^2} + V_-(x;a_0) + E_0 \tag{40}$$

From equations (34) and (40), we get:

$$V(x) = V_-(x;a_0) + E_0 = \phi^2(x,a_0) - \frac{\hbar}{\sqrt{2m}}\phi'(x,a_0) + E_0 \tag{41}$$

Where $V(x)$ is the effective potential, while superpotential $\phi(x)$ is determined hypothetically from equation (41), which is based on the shape of the effective potential of the system; after obtaining the superpotential from equation (41), then, we obtain the SUSY Hamiltonian and its effective potential of H_-.

Inspired by the construction of the semiclassical WKB quantization condition, we obtain the SWKB quantization condition for the Supersymmetric Hamiltonian H_- as follows:

$$\int_a^b \left[2m\left\{E_n^{(-)} - \phi^2(x) + \frac{\hbar}{\sqrt{2m}}\phi'(x)\right\}\right]^{1/2} dx = (n+\tfrac{1}{2})\pi\hbar \tag{42}$$

By expanding the left side of equation (42) in the power of $\hbar$ we have (Ikhdair & Hamzani, 2012):

$$\int_a^b \left[2m\left\{E_n^{(-)} - \phi^2(x)\right\}\right]^{1/2} dx + \frac{\hbar}{2}\int_a^b \frac{d\phi}{\left\{E_n^{(-)} - \phi^2(x)\right\}^{1/2}} = (n+\tfrac{1}{2})\pi\hbar \tag{43}$$

Since the first term of equation (43) has the condition where $-\phi(a) = \phi(b) = \sqrt{E_n^{(-)}}$, then,

$$\frac{\hbar}{2}\int_a^b \frac{d\phi}{\left\{E_n^{(-)}-\phi^2(x)\right\}^{1/2}} = \frac{\hbar}{2}\left\{sin^{-1}\frac{\phi(b)}{\left(E_n^{(-)}\right)^{1/2}} - sin^{-1}\frac{\phi(a)}{\left(E_n^{(-)}\right)^{1/2}}\right\} = \frac{1}{2}\hbar\pi \quad (44)$$

Equation (44) is inserted into equation (43) to yield the SWKB quantization condition as:

$$\int_a^b \left\{2m\left[E_n^{(-)} - \phi^2(x)\right]\right\}^{1/2} dx = n\pi\hbar \quad (45)$$

In equation (45), if n = 0, then $E_0^{(-)} = 0$, the two turning points coincide; therefore, SWKB is exact by construction.

RESULTS AND DISCUSSION

1. The Energy of the Scarf and Morse Non-central Potentials in the Presence of the External Magnetic and Electric Field

To obtain the energy eigenvalue of the system with the Scarf non-central and Morse potentials, the ground state energy and the superpotential in the *z*-direction are obtainable from equations (24) and (41). Equation (41) is rewritten as:

$$V_{eff} = \phi^2 - \frac{\hbar}{\sqrt{2M}}\phi' + E_0' \quad (46)$$

By applying the effective Morse potential in equation (24), the superpotential in the z direction is given as:

$$\phi(z) = -\sqrt{A}e^{-\alpha_z z} + \left(\frac{T}{2\sqrt{A}} - \frac{\hbar\alpha_z}{2\sqrt{2M}}\right) \quad (47)$$

Its ground state energy is given as:

$$E_{0z}' = -\left(\frac{T}{2\sqrt{A}} - \frac{\hbar\alpha_z}{2\sqrt{2M}}\right)^2 \quad (48)$$

The *z* part of the energy of the system is obtained by the SWKB quantization condition expressed in equation (45) that may be reduced into integral form as follows:

$$I(a,b) = \int_a^b \{(y-a)(b-y)\}^{1/2}\frac{dy}{y} = \frac{\pi}{2}(a+b) - \pi\sqrt{ab} \quad (49)$$

If equation (47) is inserted into equation (45), we have:

$$\int_{x_A}^{x_B}\sqrt{\left\{2M\left[\begin{array}{c}2ME'^{(-)}_n - \\ Ae^{-2\alpha_z z} - \\ 2\sqrt{A}\left(\frac{T}{2\sqrt{A}} - \frac{\hbar\alpha_z}{2\sqrt{2M}}\right)e^{-\alpha_z z} \\ +\left(\frac{T}{2\sqrt{A}} - \frac{\hbar\alpha_z}{2\sqrt{2M}}\right)^2\end{array}\right]\right\}} dz = n\pi\hbar \quad (50)$$

and by taking a transformation of variable in equation (50) as:

$$e^{-\alpha_z z} = y = f(z), \text{ and } dz = -\frac{dy}{\alpha_z y} \quad (51)$$

then equations (50) become:

$$\int_{x_A}^{x_B}\sqrt{2MA}\sqrt{\left\{\begin{array}{c}\frac{E'^{(-)}_n}{A} - y^2 + \\ 2\left(\frac{T}{2A} - \frac{\hbar\alpha_z}{2\sqrt{2MA}}\right)y - \\ \frac{1}{A}\left(\frac{T}{2\sqrt{A}} - \frac{\hbar\alpha_z}{2\sqrt{2M}}\right)^2\end{array}\right\}}\left(-\frac{dy}{y}\right) = n\pi\hbar\alpha_z \quad (52)$$

By comparing equations (49) and (52), we obtain the integration result of equation (52) as:

$$\sqrt{2MA}\left\{\pi\left(\frac{T}{2A} - \frac{\hbar\alpha_z}{2\sqrt{2MA}}\right) - \pi\sqrt{\frac{1}{A}\left(\frac{T}{2\sqrt{A}} - \frac{\hbar\alpha_z}{2\sqrt{2M}}\right)^2 - \frac{E'^{(-)}_n}{A}}\right\} = -n\pi\hbar\alpha_z \quad (53)$$

And we obtain:

$$\left\{\left(\frac{T\sqrt{2M}}{2\sqrt{A}} - \frac{\hbar\alpha_z}{2}\right) + n\hbar\alpha_z\right\}^2 = \left(\frac{T\sqrt{2M}}{2\sqrt{A}} - \frac{\hbar\alpha_z}{2}\right)^2 - 2ME'^{(-)}_n \quad (54)$$

From equations (48) and (54), we obtain:

$$E'_{nz} = -\left(\left(\frac{T}{2\sqrt{A}} - \frac{\hbar\alpha_z}{2\sqrt{2M}}\right) + \frac{n_z\hbar\alpha_z}{\sqrt{2M}}\right)^2 \quad (55)$$

And we find the energy eigenvalue in the *z*-direction as given by equations (23) and (55):

$$E_{nz} = -\left(\left(\frac{T}{2\sqrt{A}} - \frac{\hbar\alpha_z}{2\sqrt{2M}}\right) + \frac{n_z\hbar\alpha_z}{\sqrt{2M}}\right)^2 + \frac{(C-D)D_0}{4} - \frac{eF}{\alpha_z} - eFz_0 \quad (56)$$

that can be rewritten to be:

$$E_z = G - \left(\frac{\hbar\alpha_z}{M}\right)^2 (K + n_z)^2 \quad (57)$$

$$G = \frac{(C-D)D_0}{4} - \frac{eF}{\alpha_z} - eFz_0;$$
$$K = \frac{M}{\hbar\alpha_z}\left(\frac{T}{2\sqrt{A}} - \frac{\hbar\alpha_z}{2\sqrt{2M}}\right) \quad (58)$$

The solution of the radial part of the Schrodinger equation is obtained by setting the new parameter $\frac{eB}{Mc} = \omega_c$, ω_c is the cyclotron frequency, *M* is the effective mass of the electron, *C* and *D* are parameters of confinement potential associated with the strength of depth of potential, *B* is the external magnetic field acting on the quantum system, *m* is the magnetic quantum number. By rewriting equation (11) as:

$$\frac{\hbar^2}{2M} f''_{mn} - \left[\frac{M\omega_c^2}{8}\rho^2 + \left(\frac{C+D-(1-4m^2)\hbar^2/2M}{4\rho^2}\right)\right] f_{mn} + \left(E_\rho - \left(\frac{\hbar m\,\omega_c}{4}\right)\right) f_{mn} = 0 \quad (59)$$

and by setting new parameters in equation (59) as:

$$E'_\rho = \left(E_\rho - \frac{\hbar^2}{2M}\left(\frac{meB}{2\hbar c}\right)\right); \qquad \frac{eB}{Mc} = \omega_c;$$
$$\frac{\omega_c^2}{8} = \frac{\omega^2}{2} \rightarrow \frac{\omega_c}{2} = \omega \quad (60)$$

$$\frac{\hbar^2}{2M} \qquad l'(l'+1) = \left(\frac{C+D-(1-4m^2)\hbar^2/2M}{4}\right) \rightarrow$$
$$l' = -\frac{1}{2} + \sqrt{m^2 + \frac{2M}{\hbar^2}\left(\frac{C+D}{4}\right)} \quad (61)$$

Then equation (59) reduces to:

$$\frac{\hbar^2}{2M} f''_{mn} - \left[\frac{M\omega^2}{2}\rho^2 + \frac{\hbar^2}{2M}\left(\frac{l\prime(l'+1)}{\rho^2}\right)\right] f_{mn} + E'_\rho f_{mn} = 0 \quad (62)$$

From equations (46) and (62) we have:

$$\frac{M\omega^2}{2}\rho^2 + \frac{\hbar^2}{2M}\left(\frac{l\prime(l'+1)}{\rho^2}\right) = \phi^2(\rho) - \frac{\hbar}{\sqrt{2M}}\phi'(\rho) + \varepsilon'_0 \quad (63)$$

Where $\phi(\rho)$ is the hypothetic super potential, and ε'_0 is the ground state energy in the radial direction. By letting a super potential $\phi(\rho)$, which is constructed from the general potential equation (53), into equation (63), has the form of:

$$\phi(\rho) = A\rho + \frac{B}{\rho} \quad (64)$$

Then, from equations (63)-(64), we obtain the ground state energy and the superpotential equation as:

$$\phi(\rho) = \sqrt{\frac{M}{2}}\,\omega\rho - \frac{\hbar(l\prime+1)}{\rho\sqrt{2M}}; \varepsilon'_0 = \hbar\omega\left(l' + \frac{3}{2}\right) \quad (65)$$

Similar to the z part, the energy spectra of the radial part are also determined using the supersymmetry quantization condition given in equation (45) by setting a new variable:

$$\rho^2 = y = f(\rho) \rightarrow 2\rho d\rho = dy\ , \quad d\rho = \frac{dy}{2\sqrt{y}} \quad (66)$$

Then the superpotential in equation (65) is inserted into equation (45), and we have:

$$\int_{\rho_A}^{\rho_B} \sqrt{\left\{2M\left[E_{n_\rho}^{\prime(-)} - \left(\sqrt{\frac{M}{2}}\,\omega\rho - \frac{\hbar(l\prime+1)}{\rho\sqrt{2M}}\right)^2\right]\right\}} d\rho = n\pi\hbar \quad (67)$$

By using equations (66)-(67), we get:

$$\int_{y_A}^{y_B} M\omega \sqrt{\left\{\left[\left(\frac{2E_{n_\rho}^{(-)}}{M\omega^2} + \frac{2\hbar(l'+1)}{M\omega}\right)y - y^2 - \frac{\hbar^2(l\prime+1)^2}{M^2\omega^2}\right]\right\}} \frac{dy}{y} = 2n_\rho\pi\hbar \quad (68)$$

And by comparing equations (49) and (68), we can write:

$$M\omega\left\{\frac{\pi}{2}\left(\frac{2E_{n_\rho}^{\prime(-)}}{M\omega^2} + \frac{2\hbar(l'+1)}{M\omega}\right) - \pi\sqrt{\frac{\hbar^2(l\prime+1)^2}{M^2\omega^2}}\right\} = 2n_\rho\pi\hbar \quad (69)$$

From equation (69), we have:

$$E_{n_\rho}^{\prime(-)} = 2n_\rho\hbar\omega \quad (70)$$

Using equations (65) and (70), the radial energy spectra obtained as:

$$E_\rho = E_{n\rho} = \begin{Bmatrix} \hbar\omega\left(2n_\rho + l' + \frac{3}{2}\right) + \\ \frac{\hbar^2}{2M}\left(\frac{meB}{2\hbar c}\right) \end{Bmatrix} \quad (71)$$

By applying equation (61) to equation (71), we obtain:

$$E_{n\rho} = \hbar\frac{eB}{Mc}\left(n_\rho + \frac{1}{2}\left(\sqrt{m^2 + \frac{2M}{\hbar^2}\left(\frac{C+D}{4}\right)}\right) + \frac{1}{2}\right) + \frac{\hbar^2}{2M}\left(\frac{meB}{2\hbar c}\right) \quad (72)$$

Equation (72) can be simplified as:

$$E_{n\rho} = \hbar\frac{eB}{Mc}\left(P + n_\rho\right) + \frac{\hbar^2}{2M}\left(\frac{meB}{2\hbar c}\right) \quad (73)$$

With:

$$P = \frac{1}{2}\left(\sqrt{m^2 + \frac{2M}{\hbar^2}\left(\frac{C+D}{4}\right)}\right) + \frac{1}{2} \quad (74)$$

Then, the total energy spectra of the system are obtained from equations (56), (57), and (72) given by:

$$E(\rho,z) = E_\rho + E_z = \frac{\hbar^2}{2M}\left(\frac{meB}{2\hbar c}\right) + \hbar\frac{eB}{Mc}\left(P + n_\rho\right) + G - \left(\frac{\hbar\alpha_z}{M}\right)^2 (K + \mathrm{n}_z)^2 \quad (75)$$

The total energy of the system is expressed in equation (75).

The analysis of the energy eigenvalue for this study is compared to the closest research conducted by Khordad and Sedehi (Khordad & Sedehi, 2018) since there is no experimental data that is the same as the parameter used in this system. In Khordad and Sedehi, the ring-shaped oscillator, which is also called the Scarf noncentral potential and spherical harmonic oscillator, is given as:

$$V(r,\theta) = \frac{1}{2}m^*{\omega_0}^2r^2 + \frac{\hbar^2}{2m^*}\left(\frac{B}{r^2sin^2\theta} + \frac{C}{r^2cos^2\theta}\right) \quad (76)$$

$$V(r,\theta) = V(\rho,z) = \frac{1}{2}m^*{\omega_0}^2(\rho^2 + z^2) + \frac{\hbar^2}{2m^*}\left(\frac{B}{\rho^2} + \frac{C}{z^2}\right) \quad (77)$$

In this work, based on Figure 1, we apply Scarf non-central potential:

$$V(r,\theta) = \frac{a}{r^2sin2\theta} + \frac{bcos2\theta}{r^2sin2\theta} \quad (78)$$

$$V(r,\theta) = \frac{a}{4r^2sin^2\theta cos^2\theta} + \frac{b\left(2cos^2\theta - 1\right)}{4r^2sin^2\theta cos^2\theta} \quad (79)$$

$$V(r,\theta) = \frac{a+b}{4r^2sin^2\theta} + \frac{a-b}{4r^2cos^2\theta} \quad (80)$$

$$V(\rho,z) = \frac{a+b}{4\rho^2} + \frac{a-b}{4z^2} \quad (81)$$

Combined with Morse potential:

$$V(z) = -2D_e e^{-\alpha_z(z-z_0)} + D_e e^{-2\alpha_z(z-z_0)} \quad (82)$$

Such that we have the applied potential given as:

$$V(\rho,z)=\frac{a+b}{4\rho^2}+\frac{a-b}{4z^2}-2D_e e^{-\alpha_z(z-z_0)}+D_e e^{-2\alpha_z(z-z_0)} \quad (83)$$

A similar condition has also been studied (Khordad & Sedehi, 2018). They solved the Schrodinger equation under the influence of the magnetic field with a ring-shaped oscillator and a spherical harmonic oscillator potential. At this point, we can compare the calculation result in this work to that obtained in the reference (Khordad & Sedehi, 2018) to check the correctness of the mathematical calculations, including the derivation of the differential Schrodinger equation, so that the obtained solutions will be more accurate. By comparing the radial part of Schrodinger equation (5) in Ref. (Khordad & Sedehi, 2018) written as:

$$\frac{d^2F(z)}{dz}-\left[\frac{m^{*2}\omega_0^2}{\hbar}z^2+\frac{C}{z^2}-\frac{2m^*E_z}{\hbar^2}-\frac{2m^*}{\hbar^2}eFz\right]F(z)=0$$

With the radial part of the Schrodinger equation expressed in equation (59) in this work, it is shown that the two equations have similar effective potential but with different notation of parameters, such as they denoted the external magnetic by Ω and the potential parameter by B and C. In contrast, in this work, the external magnetic is denoted by B and the potential parameter by C and D. Besides, we used the Scarf non-central potential with the influence of magnetic field in this study for the ρ-part where it is reduced into the form of inverse square potential and Morse potential for the z-part. Whereas Khordad and Sedehi (2018), for the ρ-part, used the addition of oscillator harmonic potential, and for the z-part, they used modified square and inverse square potential.

Moreover, the energy equation of ρ-part expressed in equation (73) is similar to the energy equation of the reference with different parameters. Due to the similarity in the second-order differential equation of the Schrodinger equation, the effective potential, and the energy equation (although the parameter used is different), the computational and numerical results can be compared to the data proved by Khordad and Sedehi (2017).

Using equation (75), the energy eigenvalue of diatomic molecules in Table 1 is numerically calculated with the variation of quantum number n, magnetic field B, and electric field F. In this case, the effective mass of the molecules is presented in Table 1. We use a natural unit for the other parameters to simplify the computational process without changing the results, as follows $m=0,\hbar=e=c=1,De=3$.

Table 2 shows the energy eigenvalue as a quantum number (n) function for four cases with three different diatomic molecules with the mass parameter taken from Table 1. The energy increases as the quantum number is raised for each case and also increases due to the external magnetic field B. The change in the electric field F doesn't significantly affect the energy eigenvalue of the system.

Table 1. Molecular Parameter (Faniandari Et Al., 2022)

Molecule	M (amu)
Hydrogen (H_2)	0.5039100
Lithium hydride (LiH)	0.8801221
Hydrogen chloride (HCl)	0.9801045

Table 2. The energy eigenvalues for the Scarf and Morse potentials under the influence of B and F with various n for parameters $C=0.5$, $D=0.1$, and $\alpha=0.05$

n	F (T)	B (T)	E (eV)		
			H_2	LiH	HCl
1	0	0	159.850	80.227	69.695
	0	2	166.575	84.219	73.309
	2	0	159.841	80.218	69.687
	2	2	166.566	84.211	73.301
2	0	0	377.161	204.654	181.430
	0	2	387.855	210.918	187.085
	2	0	377.147	204.643	181.420
	2	2	387.841	210.908	187.075
3	0	0	594.451	329.074	293.160

n	F (T)	B (T)	E (eV)		
			H_2	LiH	HCl
	0	2	609.114	337.611	300.855
	2	0	594.434	329.062	293.148
	2	2	609.097	337.599	300.843
4	0	0	811.722	453.488	404.884
	0	2	830.354	464.298	414.620
	2	0	811.702	453.473	404.871
	2	2	830.334	464.283	414.607

We can't compare our results because the reference does not calculate the energy level numerically. However, the similarity in the form of the energy equation caused the partition function and the other thermodynamic properties to have a similar form to the reference (Khordad & Sedehi, 2017). So, the other thermodynamic properties can be compared with the previous research.

2. The Thermodynamics and Magnetic Properties of the Scarf Non-central and Morse Potentials in the Presence of the External Electric and Magnetic Field

Thermodynamical and magnetic properties of a quantum system influenced by Scarf hyperbolic and Morse confinement potentials are determined using the energy spectra expressed in equation (75). In the classical regimes (Edet et al., 2021), the nonrelativistic energy equation in equation (75) yields the vibrational partition function, internal energy, specific heat, and entropy. The vibrational partition function is given as (Bera et al., 2019; Edet et al., 2021; Khordad et al., 2019; Khordad & Sedehi, 2018; Okorie, Edet, et al., 2020):

$$Z(\zeta,\beta)=\sum_{n=0}^{\zeta} e^{-\beta E_{nl}}, \beta=\frac{1}{kT} \tag{84}$$

k is the Boltzmann constant, E_n is the nonrelativistic energy spectrum (in eV). Then, the partition function is obtained directly from equation (75) given (Edet et al., 2021):

$$Z(\beta)=Z_\rho(\beta)+Z_z(\beta)$$
$$=\{e^{-\beta\left(\frac{\hbar^2}{2M}\left(\frac{meB}{2\hbar c}\right)+G\right)}\sum_{\mathrm{n}_z}^{\mathrm{n}_{zmax}} e^{\beta\left(\frac{\hbar\alpha_z}{M}\right)^2(K+\mathrm{n}_z)^2}$$
$$\sum_{n_\rho}^{n_{\rho max}} e^{-\beta\hbar\omega_c(P+n_\rho)}\} \tag{85}$$

The radial and z-part of the partition function can be rewritten as:

$$Z_\rho(\beta)=e^{-\beta\hbar\omega_c P}\sum_{n_\rho}^{n_{\rho max}} e^{-\beta\hbar\omega_c(n_\rho)}=\frac{e^{-\beta\hbar\frac{eB}{Mc}P}}{1-e^{-\beta\hbar\frac{eB}{Mc}}} \tag{86}$$

$$Z_z(\beta)=\frac{M}{\hbar\alpha_z\sqrt{\beta}}\frac{\sqrt{\pi}}{2}\left\{erfi\left(\sqrt{\beta}\frac{\hbar\alpha_z}{M}K\right)\right\} \tag{87}$$

By using equations (84-87), the total partition function of the quantum system becomes:

$$Z(\beta)=e^{-\beta\left(\frac{\hbar^2}{2M}\left(\frac{meB}{2\hbar c}\right)+G\right)}\frac{e^{-\beta\hbar\frac{eB}{Mc}P}}{1-e^{-\beta\hbar\frac{eB}{Mc}}}\frac{M}{\hbar\alpha_z\sqrt{\beta}}\frac{\sqrt{\pi}}{2}\left\{erfi\left(\sqrt{\beta}\frac{\hbar\alpha_z}{M}K\right)\right\} \tag{88}$$

Where:

$$K=\frac{M}{\hbar\alpha_z}\left(\frac{T}{2\sqrt{A}}-\frac{\hbar\alpha}{2\sqrt{2M}}\right);\ G=\frac{(C-D)D_0}{4}-\frac{eF}{\alpha_z};$$
$$P=\frac{1}{2}\left(\sqrt{m^2+\frac{2M}{\hbar^2}\left(\frac{C+D}{4}\right)}\right)+\frac{1}{2} \tag{89}$$

And:

$$erf(x)=\frac{2}{\sqrt{\pi}}\int_0^x e^{-t^2}dt;\ erfi(x)=\frac{2}{\sqrt{\pi}}\int_0^x e^{t^2}dt \tag{90}$$

By applying equations (84-90), we obtain the partition function of the system written as:

$$Z(\beta)=\frac{e^{-\beta\left(\left(\frac{\hbar eB}{Mc}\right)\left(\frac{m}{4}+P\right)+G\right)}}{1-e^{-\beta\hbar\frac{eB}{Mc}}}\frac{M}{\hbar\alpha_z\sqrt{\beta}}\frac{\sqrt{\pi}}{2}\left\{erfi\left(\sqrt{\beta}\frac{\hbar\alpha_z}{M}K\right)\right\} \tag{91}$$

The partition function expressed in equation (91) is used to calculate numerically internal energy, specific heat, free energy, entropy, magnetization, magnetic susceptibility at finite and zero temperature, persistent current, and delta entropy defined as follows (Edet & Ikot, 2021; Edet et al., 2021):

1. Vibrational mean energy/internal energy

$$U(\beta) = -\frac{1}{Z(\beta)}\frac{\partial Z(\beta)}{\partial \beta} \tag{92}$$

2. Specific free capacity

$$C(\beta) = -k\beta^2\frac{\partial U}{\partial \beta} \tag{93}$$

3. Free energy

$$F(\beta) = -kT\, ln\, Z_{vib}\,(\beta) \tag{94}$$

4. Entropy

$$S(\beta) = -k\beta\frac{\partial F}{\partial \beta} \tag{95}$$

5. Magnetization at finite temperature

$$M'(\beta) = \frac{1}{\beta}\left(\frac{1}{Z(\beta)}\right)\frac{\partial Z(\beta)}{\partial B} \tag{96}$$

6. Magnetization at zero temperature

$$M'(\beta) = -\frac{\partial E(\rho,z)}{\partial B} \tag{97}$$

7. Magnetic susceptibility

$$\chi_m(\beta) = \frac{\partial M\prime(\beta)}{\partial B} \tag{98}$$

8. Persistent current

$$I = \left[-\frac{e}{\hbar c}\right]\frac{\partial F(\beta)}{\partial M} \tag{99}$$

9. Delta entropy

$$\Delta S = S(B \neq 0, T) - S(B = 0, T) \tag{100}$$

The vibrational mean energy of the quantum system is obtained by using equation (92) as:

$$U(\beta) = \left(\left(\frac{\hbar eB}{Mc}\right)\left(\frac{m}{4}+P\right)+G\right) + \frac{\left(\hbar\frac{eB}{Mc}\right)}{-1+e^{\beta\hbar\frac{eB}{Mc}}} + \frac{1}{2\beta} - \frac{\left\{\frac{\hbar\alpha_z K}{\mathrm{M}\sqrt{\beta}\sqrt{\pi}}e^{\frac{\beta\hbar^2\alpha_z^2K^2}{M^2}}\right\}}{\left\{erfi\left(\sqrt{\beta}\frac{\hbar\alpha_z}{M}K\right)\right\}} \tag{101}$$

The specific heat of the quantum system is found by using equation (93) as:

$$C(\beta) = -k\beta^2\left\{-\frac{\left(\hbar\frac{eB}{Mc}\right)^2 e^{\beta\hbar\frac{eB}{Mc}}}{\left(-1+e^{\beta\hbar\frac{eB}{Mc}}\right)^2} + \frac{1}{2\beta^2} - \frac{\hbar\alpha_z K e^{\frac{\beta\hbar^2\alpha_z^2K^2}{M^2}}}{erfi\left(\sqrt{\beta}\frac{\hbar\alpha_z}{M}K\right)\mathrm{M}\sqrt{\beta\pi}}\left(\left(-\frac{1}{2\beta}+\frac{\hbar^2\alpha_z^2K^2}{M^2}\right)\right) + \frac{(\hbar\alpha_z K)^2}{\left\{erfi\left(\sqrt{\beta}\frac{\hbar\alpha_z}{M}K\right)\right\}^2\mathrm{M}^2\beta\pi}e^{\frac{2\beta\hbar^2\alpha_z^2K^2}{M^2}}\right\} \tag{102}$$

The vibrational free energy (F) of the quantum system is obtained by using equation (94) as:

$$F(\beta) = -\frac{1}{\beta}ln\left(\frac{e^{-\beta\left(\left(\frac{\hbar eB}{Mc}\right)\left(\frac{m}{4}+P\right)+G\right)}}{1-e^{-\beta\hbar\frac{eB}{Mc}}}\frac{M}{\hbar\alpha_z\sqrt{\beta}}\frac{\sqrt{\pi}}{2}\left\{erfi\left(\sqrt{\beta}\frac{\hbar\alpha_z}{M}K\right)\right\}\right) \tag{103}$$

and equation (95) is used to arrive the following vibrational entropy (S) of the quantum system:

$$S(\beta) = -k\beta\left\{\left(\frac{1}{\beta^2}ln\, Z_{vib}\,(\beta)\right) + \frac{1}{\beta}\left(\left(\frac{\hbar eB}{Mc}\right)\left(\frac{m}{4}+P\right)+G\right) + \frac{\left(\hbar\frac{eB}{Mc}\right)}{-1+e^{\beta\hbar\frac{eB}{Mc}}} + \frac{1}{2\beta} - \frac{\left\{\frac{\hbar\alpha_z K}{\mathrm{M}\sqrt{\beta}\sqrt{\pi}}e^{\frac{\beta\hbar^2\alpha_z^2K^2}{M^2}}\right\}}{\left\{erfi\left(\sqrt{\beta}\frac{\hbar\alpha_z}{M}K\right)\right\}}\right\} \tag{104}$$

Then, by using equation (97), the magnetization at finite temperature M', is given by:

$$M'(\beta) = -\left(\frac{\hbar e}{Mc}\right)\left\{\left(P+\frac{m}{4}\right)+\frac{1}{\left(e^{\beta\hbar\frac{eB}{Mc}}-1\right)}\right\} \quad (105)$$

The magnetization at zero temperature is obtained by using equation (97):

$$M'(\beta) = -\frac{\hbar e}{Mc}\left\{\left(\frac{m}{4}\right)+\left(P+n_\rho\right)\right\} \quad (106)$$

The susceptibility of the system at zero temperature is:

$$\chi_m(\beta) = 0 \quad (107)$$

The magnetic susceptibility of the system at a finite temperature is obtained by using equations (98) and (96) as follows:

$$\chi_m(\beta) = \frac{\left(\frac{\hbar e}{Mc}\right)\beta\frac{\hbar e}{Mc}e^{\beta\hbar\frac{eB}{Mc}}}{\left(e^{\beta\hbar\frac{eB}{Mc}}-1\right)^2} = \frac{\left(\frac{\hbar e}{Mc}\right)\beta\frac{\hbar e}{Mc}}{4sinh^2\left(\beta\hbar\frac{eB}{2Mc}\right)} \quad (108)$$

By using equation (97), the persistent current is found to be:

$$I(\beta) = \left[-\frac{e}{hc}\right]\left[-\frac{1}{\beta}\right]\left[-\frac{\beta\hbar eB}{4Mc}\left(1+\frac{m}{P-\frac{1}{2}}\right)\right] = -\frac{Be^2}{8\pi Mc^2}\left(1+\frac{m}{P-\frac{1}{2}}\right) \quad (109)$$

We simulate each of the thermodynamic and magnetic properties as a function of temperature function $\beta = \frac{1}{T}$, electric field F(T), and magnetic field B(T). Figure 2 shows the plot of the partition function of the Scarf and Morse potentials with the variation of mass M: (a) as a function of β, (b) as a function of F, and (c) as a function of B. In Figure 2(a), it can be observed that the partition function decreases with the increasing temperature function β. So, it decreases as the temperature value increases. Figure 2(b) shows that the partition function increases with an increase in the electric field parameter F. Figure 2(c) indicates that the partition function decreases with an increase in the magnetic field parameter B.

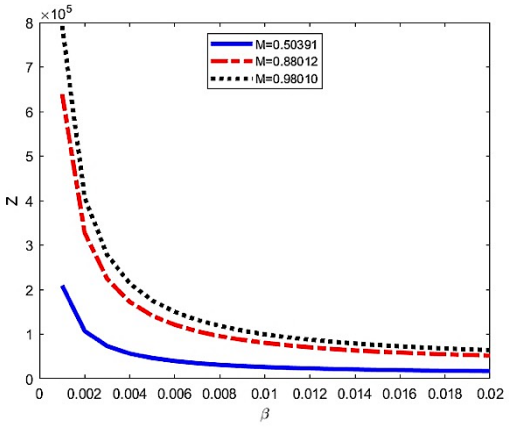

(a)

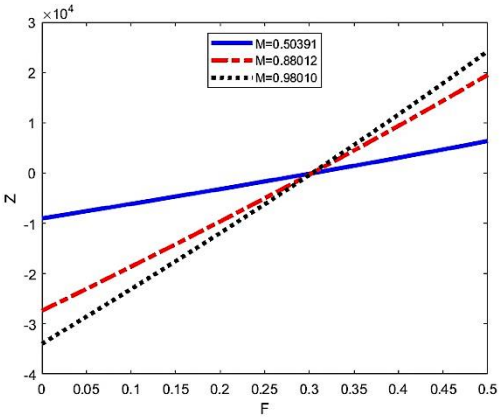

(b)

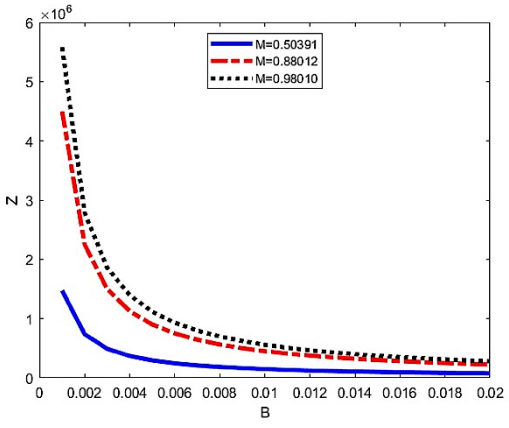

(c)

Figure 2. (a) The Plot of Partition Function as a Function of (a) β (b) F (c) B for Different Values of M

From Figures 2(a) and 2(c), it is concluded that the Z function reaches

saturation values for low temperature and high magnetic field values regardless of the mass parameter M. Meanwhile, from Figure 2(b), it is clear that the higher mass parameter M has a more significant effect on the Z-function. The partition function simulates the distribution of the energy of particles. The plot of the Z-function in Figure 2(b) shows the linear trend.

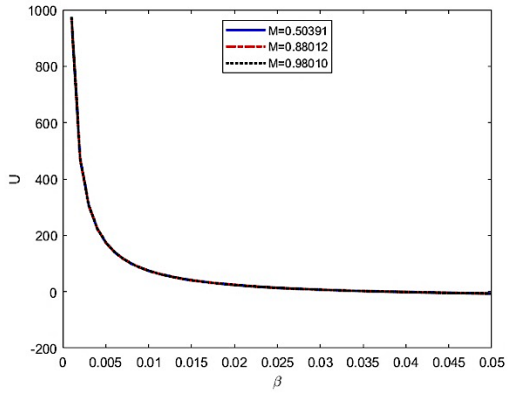

(a)

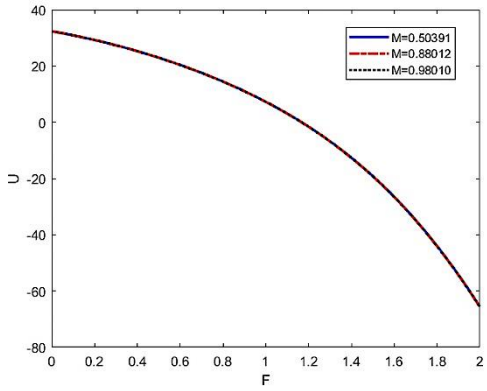

(b)

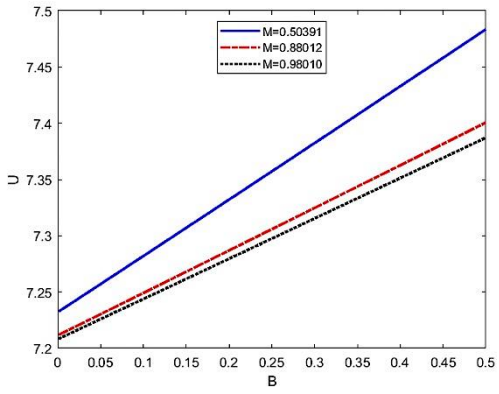

(c)

Figure 3. (a) The Plot of Internal Energy as a Function of (a) β (b) F (c) B for Different Values of M.

Figure 3 shows the plot of the internal energy of the Scarf and Morse potentials with the variation of mass M (a) as a function of β, (b) as a function of F, and (c) as a function of B. In Figure 3(a), it can be seen that the internal energy exhibits saturation. As the β increases, the internal energy reaches a limit. The internal energy decreases with the increase of the electric field parameter F in Figure 3(b), and it enhances linearly with increasing the magnetic field parameter B in Figure 3(c). The decrease in temperature and magnetic field causes the internal energy to increase so that the motion of the molecules will be more stable since the internal energy corresponds to the potential energy and kinetic energy in the vibrational motion of the molecules. The results in Figure 3 show that the internal energy is insensitive to changes in the M parameter. It is highly sensitive to the applied magnetic field changes and slightly sensitive to the β and F parameters. The internal energy results are compared to the reference (Khordad & Sedehi, 2018). It is found that Figure 3(a) is similar to the internal energy depicted in Khordad and Sedehi, which increases with the increase of temperature T. It should be noted that in this work, we simulate the internal energy with the temperature function β, where $\beta = \frac{1}{kT}$.

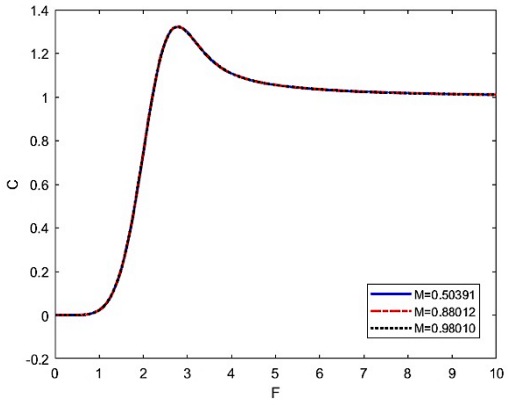

(a)

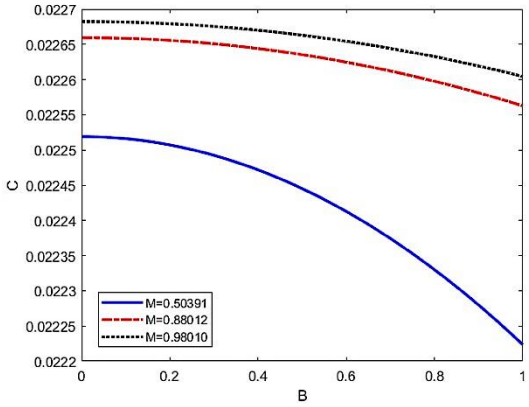

(b)

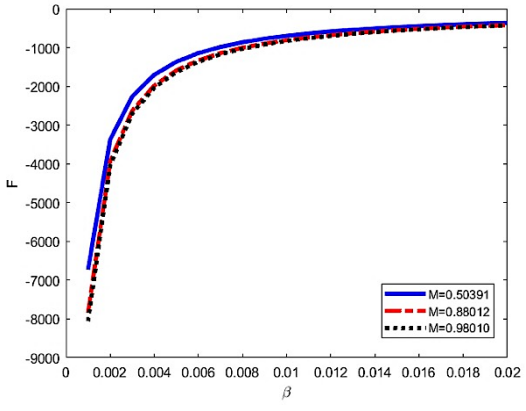

(a)

Figure 4. (a) The plot of the Specific Heat Capacity as a Function of (a) F and (b) B for Different Val

Figure 4 shows the plot of the specific heat capacity of the Scarf and Morse potentials with the variation of mass parameter M (a) as a function of electric field parameter F and (b) as a function of external magnetic field parameter B. Figure 4(a) shows that the specific heat capacity increases and then decreases with an increase in the F parameter. Figure 4(b) shows that the specific heat capacity reduces with increasing B. The results in Figure 4 allow us to infer that the specific heat capacity is sensitive to the applied magnetic field. For $F \rightarrow 0\ T$, the value of the specific heat capacity is almost zero, and it reaches the higher value of the specific heat capacity in 2T< F < 4T. For F > 4T, the specific heat capacity exhibits saturation. In this case, the specific heat capacity has a negative value. This can be interpreted as meaning that when the system vibrates, energy is lost by radiation. The specific heat capacity behaves similarly to the results (Khordad & Sedehi, 2018).

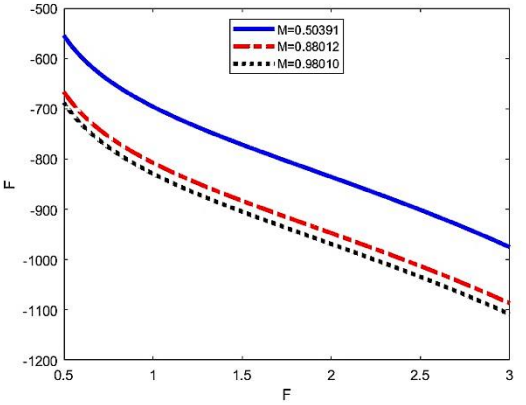

(b)

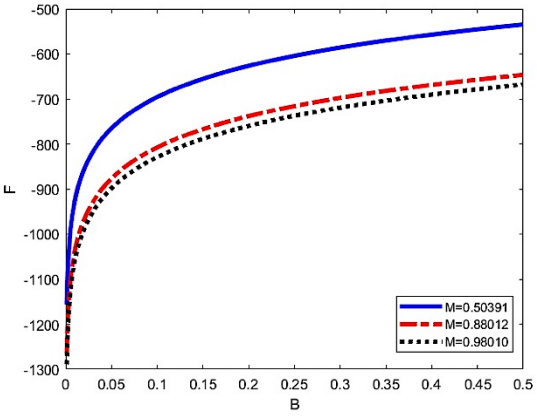

(c)

Figure 5. (a) The Plot of Free Energy as a Function of (a) β (b) F (c) B for Different Values of M

Figure 5 shows the plot of free energy of the Scarf and Morse potentials with the variation of mass parameter M (a) as a function of temperature function β, (b) as a function of electric field F, and (c) as a function of external magnetic field B. In Figure 8(a), it is observed that free energy

enhances with enhancing β. Figure 5(b) shows that free energy decreases with an increase in the F parameter. In Figure 5(c), the free energy exhibits saturation. This means that as B increases, the free energy reaches a limit. Free energy represents work outside the system that results from changes in the system's internal energy in a thermodynamic process. In this case, the system's stability is deteriorating because the value of the free energy rises as the external magnetic field B enhances, especially in regions with a strong magnetic field effect. The results of Figure 5 allow us to conclude that free energy is most sensitive to changes in the M and F parameters, slightly sensitive to the B parameter, and insensitive to temperature. We can't compare the free energy to the result (Khordad & Sedehi, 2018) since they do not obtain and simulate it numerically.

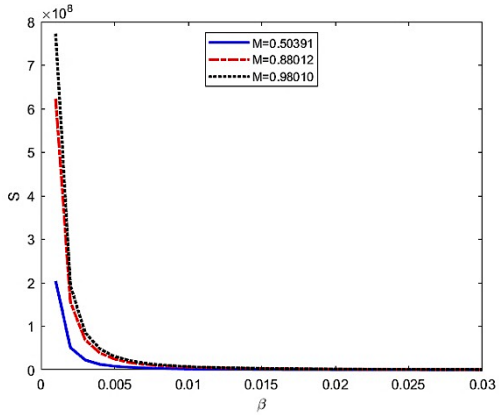

(a)

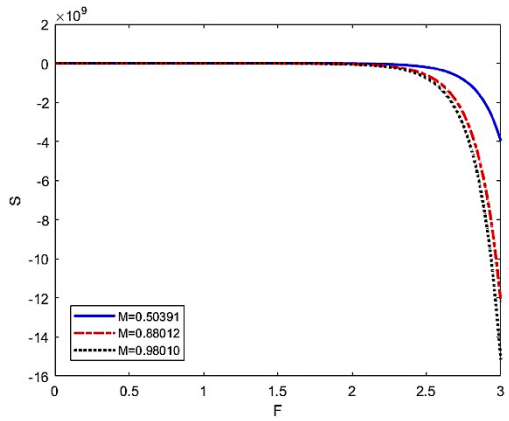

(b)

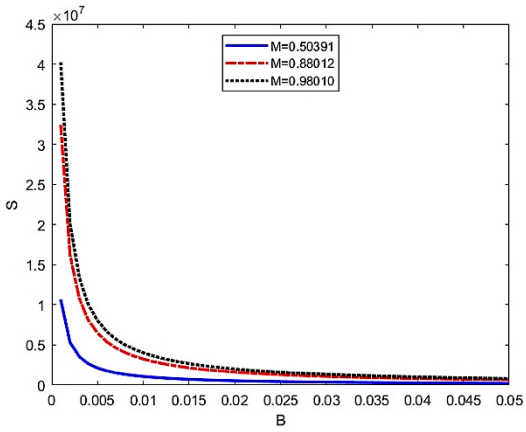

(c)

Figure 6. (a) The Plot of Entropy as a Function of (a) β (b) F (c) B for Different Values of M

Figure 6 shows the plot of entropy of the Scarf and Morse potentials with the variation of mass parameter M (a) as a function of temperature function β, (b) as a function of electric field parameter F, and (c) as a function of the external magnetic field B. Figures 6(a) and 6(c) show that the entropy highly decreases and then slightly decreases with increasing β and B, respectively. This means that the system's entropy will increase at high temperatures, and the particles will become more unstable. Figure 6(b) shows that the entropy increases with increasing F. Figure 6 shows that the entropy is equally sensitive to changes in the β, F, and B parameters. Then, the entropy in Figure 6(a) exhibits the same behavior as the entropy as a function of temperature (Khordad & Sedehi, 2018); it increases with the growth of temperature. In Figure 6(a), we plot it against the temperature function β, where $\beta = \frac{1}{kT}$, so it shows the opposite graphs.

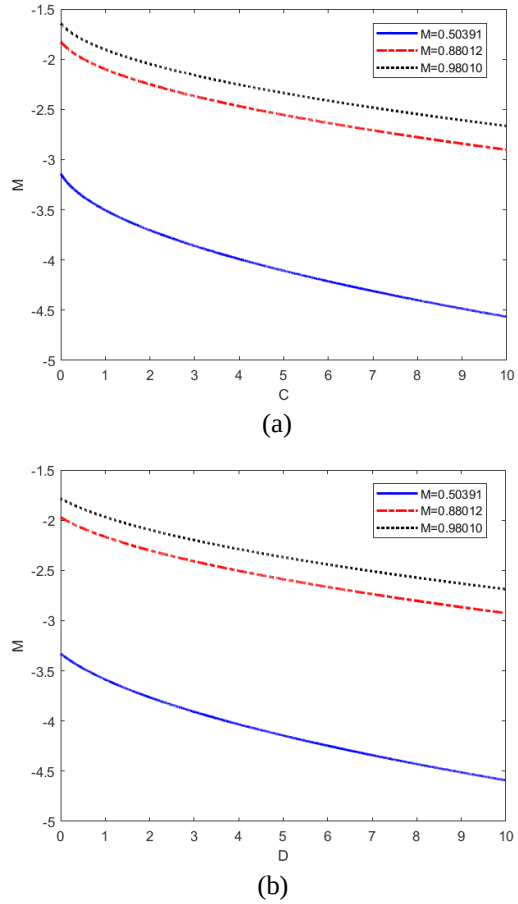

Figure 7. The Plot of Magnetization at Zero Temperature as a Function of (a) C, (b) D for Different Values of M

Figure 7 depicts the plot of magnetization of the Scarf and Morse potentials at zero temperature with the variation of mass parameter M (a) as a function of potential parameter C and (b) as a function of potential parameter D. Figures 7(a) and 7(b) show that the magnetization decreases with increasing both C and D. From Figure 7, it can be seen that the magnetization is mostly sensitive to changes in the applied C and D parameters and is essentially constant for variations in the mass parameter M.

Figure 8 shows the plot of magnetization of the Scarf and Morse potentials at finite temperature with the variation of mass parameter M (a) as a function of potential parameter C and (b) as a function of potential parameter D. The magnetization decreases with increasing both C and D as shown in Figures 8(a) and 8(b). Figures 7 and 8 show that the mass parameter M contributes to the magnetization effect. At zero temperature, the magnetization is essentially constant for variation in the mass parameter M. Meanwhile, for finite temperatures, the magnetization shows its changes in the variation of the mass parameter M, and this effect is significant in the high potential parameter C and D regimes.

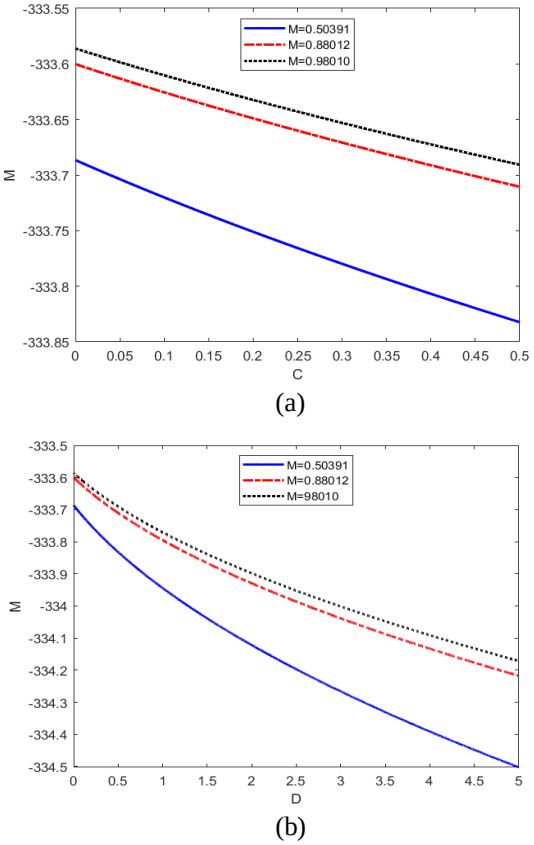

Figure 8. The Plot of Magnetization at Finite Temperature as a Function of (a) C, (b) D for Different Values of M

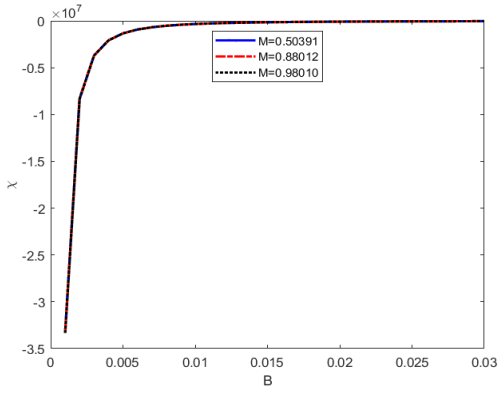

Figure 9. The Plot of Magnetic Susceptibility at Finite Temperature against B for Different Values of M

Figure 9 illustrates the magnetic susceptibility of the Scarf and Morse potentials as a function of the external magnetic field B under different mass parameters M. From Figure 9. We can see that the magnetic susceptibility decreases at the origin to almost zero point and then increases slightly with an increasing magnetic field. The magnetic susceptibility is almost constant in the region where B > 0.02T. The result is similar to the finding in (Khordad & Sedehi, 2018), where the magnetic susceptibility increases with the raising of the magnetic fields.

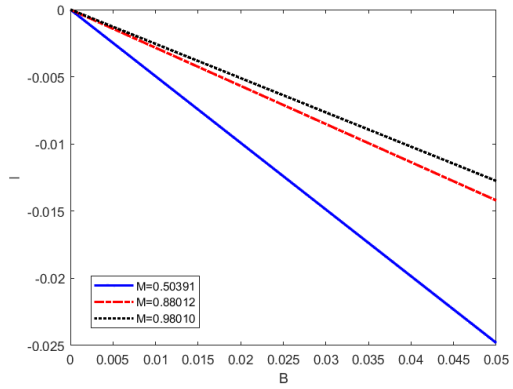

Figure 10. The Plot of the Persistent Current against B for Different Values of M

Figure 10 shows the plot of the persistent current of the Scarf and Morse potentials with the variation of mass parameter M as a function of the external magnetic field B. Figure 10 shows that the persistent current decreases linearly with increasing B, which indicates that the perpetual electric current decreases in the greater magnetic field. This result is in good agreement with the result in the ref. (Faniandari et al., 2022).

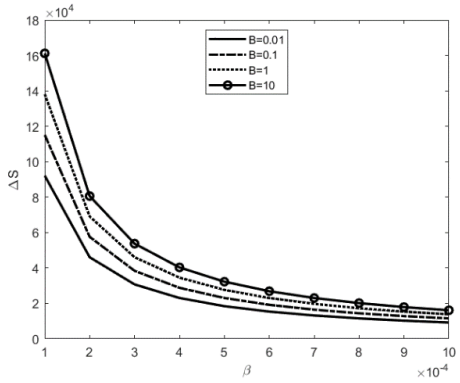

(a)

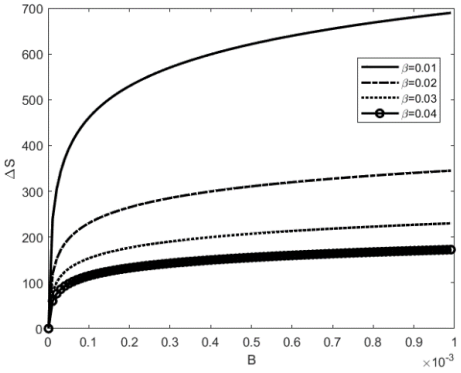

(b)

Figure 11. The Plot of Delta Entropy as a Function of (a) β (b) B

Figure 11 shows the plot of the delta entropy of the Scarf and Morse potentials with the variation of mass parameter M (a) as a function of temperature function β and (b) as a function of external magnetic field B calculated numerically by using equation (100). The delta entropy decreases with the increasing of β shown in Figure 11(a). It can be seen that the variations in delta entropy with temperature are significant at high temperatures. In Figure 11(b), the delta entropy rises with increasing B. The variations of B in the delta entropy are observed to have a small effect. However, the delta entropy has positive values, which indicates that the particle becomes more disordered.

The graphs of the thermodynamic properties of the H_2, LiH, and HCl diatomic molecules show that the behavior of the three selected diatomic molecules does not exhibit a significant difference since their rest masses have only a small difference. In contrast, the presence of the magnetic field contributes strongly to changing the system. These results are supported by research reported (Khordad & Sedehi, 2018), which shows that the different values of the magnetic field caused the thermodynamic properties to change. In addition, the magnetic properties are also examined in this work. From the results, the magnetic susceptibility of the three selected diatomic molecules has a negative value, characteristic of diamagnetic materials.

At this point, these theoretical results can be useful for some physical systems related to applications in condensed matter physics and other similar research since understanding the thermodynamic properties helps in characterizing the energy distribution and thermal behaviour.

On the other hand, in this current work, the nonrelativistic Schrodinger equation was solved using SUSYQM, so only the shape invariance potential models can be applied.

CONCLUSION AND SUGGESTION

This paper studied the effects of magnetic and electric fields on thermodynamic and magnetic properties. The SUSY method was used to obtain the energy spectra for the system. The partition function was obtained from the energy equation and used to calculate the internal energy, specific heat capacity, free energy, entropy, persistent current, and delta entropy. **F**urthermore, the magnetization and magnetic susceptibility of the system were considered at zero and finite temperatures. The energy eigenvalue increases as the magnetic field increases but decreases as the electric field increases. The enhancement of the parameter α increases the energy eigenvalue and applies to parameter C. For the parameter potential D, it is observed that the energy eigenvalue decreases as parameter D increases. The magnetic susceptibility of the system exhibits a diamagnetic behavior when plotted against B. The results of this work are compared to similar referred work, and they show consistency. These analytical expression results can be useful for research into other physical systems in condensed matter physics and related fields.

ACKNOWLEDGMENT

This research was partly supported by Sebelas Maret University under Fundamental Research Grant number 228/UN27.22/PT.01.03/2023.

REFERENCES

Abu-Shady, M., & Ikot, A. N. (2019). Analytic solution of multi-dimensional Schrödinger equation in hot and dense QCD media using the SUSYQM method. *The European Physical Journal Plus volume, 134*(321).

Ahmadov, A. I., Maria, N., Qocayeva, M. V., & Tarverdiyeva, V. A. (2018). Analytical Solutions of the Schrödinger Equation for the Manning-Rosen plus Hulthén Potential Within SUSY Quantum Mechanics. *Journal of Physics: Conference Series, 965*.

Assi, I. A., Ikot, A. N., & Chukwuocha, E. O. (2018). Solutions of the ?-Dimensional Schrödinger Equation with the Hyperbolic Pöschl-Teller Potential plus Modified Ring-Shaped Term. *Advances in High Energy Physics, 2018*, 1-10.

Bala, K. J., Peter, A. J., & Lee, C. W. (2017). Simultaneous effects of pressure and temperature on the optical transition energies in a Ga0. 7In0. 3N/GaN quantum ring. *Chemical Physics, 495*(1), 42-47.

Banger, S., Nayak, V., & Verma, U. P. (2018). Hydrogen storage in lithium hydride: A theoretical approach. *Journal of Physics and Chemistry of Solids, 115*, 6-17.

Bera, A., Ghosh, A., & Ghosh, M. (2019). Analyzing magnetic susceptibility of impurity doped quantum dots in presence of noise. *Journal of Magnetism and Magnetic Materials, 484*(1), 391-402.

Biswas, A., Pathak, A. K., Zarkevich, N. A., Xubo, L., Mudryk, Y., Balema, V., Johnson, D. D., & Pecharsky, V. K. (2019). Designed materials with the giant magnetocaloric effect near room temperature. *Acta Materialia, 180*(1), 341-348.

Castillo, D. E. A., & Kirchbach, M. (2007). Exact spectrum and wave functions

of the hyperbolic Scarf potential in terms of finite Romanovski polynomials. *Revista Mexicana de Fisica E*, *53*(2), 143-154.

Castro, P. B. D., Terashima, K., Yamamoto, T. D., Hou, Z., Iwasaki, S., Matsumoto, R., Adachi, S., Saito, Y., Song, P., Takeya, H., & Takano, Y. (2020). Machine-learning-guided discovery of the gigantic magnetocaloric effect in HoB2 near the hydrogen liquefaction temperature. *NPG Asia Materials*, *12*(1), 1-7.

Comtet, A., Bandrauk, A. D., & Campbell, D. K. (1985). Exactness of Semiclassical Bound State Energies for Supersymmetric Quantum Mechanics. *Physics Reviews D*, *36*(8).

Dabrowaska, J. W., Khare, A., & Sukhatme, P. (1988). Explicit wavefunctions for shape-invariant potentials by operator techniques. *Journal of Physics A: Mathematical and General*, *21*(4), L195-L200.

Dianawati, D. A., Suparmi, A., & Cari, C. (2019). Study of Schrodinger Equation with Quantum Deformation for Three-Dimensional Harmonic Oscillator plus Inverse Quadratic Potential by Hypergeometric Method. *International Journal of Advanced Trends in Computer Science and Engineering*, *8*(6), 2788-2793.

Dong, S., Dong, Q., Sun, G.-H., Femmam, S., & Dong, S.-H. (2018). Exact Solutions of the Razavy Cosine Type Potential. *Advances in High Energy Physics*, *2018*, 1-6.

Dutt, R., Khare, A., & Sukhatme, U. P. (1988). Supersymmetry, Shape Invariance, and Exactly Solvable Potentials. *American Journal of Physics*, *56*(2).

Edet, C. O., Amadi, P. O., Ettah, E. B., Ali, N., Asjad, M., & Ikot, A. N. (2022). The magnetocaloric effect, thermo-magnetic and transport properties of LiH diatomic molecule. *Molecular Physics*, *2022*(1).

Edet, C. O., & Ikot, A. N. (2021). Effects of Topological Defect on the Energy Spectra and Thermo-magnetic Properties of CO Diatomic Molecule. *Journal of Low Temperature Physics*, *203*(1).

Edet, C. O., Ikot, A. N., Onyeaju, M. C., Okorie, U. S., Rampho, G. J., Lekala, M. L., & Kaya, S. (2021). Thermo-magnetic properties of the screened Kratzer potential with spatially varying mass under the influence of Aharanov-Bohm (AB) and position-dependent magnetic fields. *Physica E: Low-dimensional Systems and Nanostructures,* , *131*(114710), 1-14.

Fang, J., Zhou, Z., Xiao, M., Lou, Z., Wei, Z., & Shen, G. (2019). Recent advances in low-dimensional semiconductor nanomaterials and their applications in high-performance photodetectors. *Chinese Academy of Sciences & Center of Materials Science and Optoelectronics Engineering*, *2020*, 291-317.

Faniandari, S., Suparmi, A., & Cari, C. (2022). Study of thermomagnetic properties of the diatomic particle using hyperbolic function position dependent mass under the external hyperbolic magnetic and AB force. *Molecular Physics*, *120*(12). https://doi.org/ https://doi.org/10.1080/00268976.2022.2083712

Faniandari, S., Suparmi, A., Cari, C., & Harjana, H. (2023). Study of Thermomagnetic Properties for Nonrelativistic Particle with Position Dependent Mass in the Presence of Topological Defect and External Magnetic Field: Theory and Simulation. *International Journal of Theoretical Physics*, *62*(109).

Fuhrmann, B., Leipner, H. S., Hoche, H. R., Schubert, L., Werner, P., & Gosele, U. (2005). Ordered arrays of silicon nanowires produced by nanosphere lithography and molecular beam epitaxy. *Nano Lett*, *5*(12), 2524-2527. https://doi.org/10.1021/nl051856a

Gangopadhyaya, A., Bougie, J., & Rasinariu, C. (2021). Exactness of Semiclassical Quantization Rule for Broken Supersymmetry. *Journal of Physics A: Mathematical and Theoretical*
54(29).

Gendenshtien, L. E. (1983). Derivation of exact spectra of the Schr0dinger equation by means of Supersymmetry. *Journal of Experimental and Theoretical Physics Letters*, *38*(6), 356-359.

Gschneidner, K. A., Pecharsky, V. K., & Tsokol, A. O. (2005). Recent developments in magnetocaloric materials. *Reports on progress in physics*, *68*(6), 1479-1539.

Hassanabadi, H., Chung, W. S., & Bhardwaj, S. B. (2018). ?-Deformed Morse and Oscillator Potential. *Advances in High Energy Physics*, *2017*(1-5).

Hassanabadi, H., Maghsoodi, E., Ikot, A. N., & Zarrinkamar, S. (2018). Minimal Length Schrödinger Equation with Harmonic Potential in the Presence of a Magnetic Field. *Advances in High Energy Physics*, *2013*, 1-7.

Houtot, A. (1973). Exact motion in noncentral electric fields *Journal of Mathematical Physics*, *14*(10), 1320-1327.

Ikhdair, S. M., & Falaye, B. J. (2013). Approximate analytical solutions to relativistic and nonrelativistic Pöschl–Teller potential with its thermodynamic properties. *Chemical Physics*, *421*, 84-95. https://doi.org/https://doi.org/10.1016/j.chemphys.2013.05.021

Ikhdair, S. M., & Hamzani, M. (2012). A quantum pseudodot system with two-dimensional pseudoharmonic oscillator in external magnetic and Aharonov-Bohm fields. *Physica B: Condensed Matter*, *407*(21), 4198–4207.

Ikot, A. N., Okorie, U. S., Sever, R., & Rampho, G. J. (2019). Eigensolution, expectation values and thermodynamic properties of the screened Kratzer potential. *European Physics Journal Plus*, *134*(1), 1-18.

Jia, C. S., Zhang, L.-H., Peng, X.-L., Luo, J.-X., Zhao, Y.-L., Liu, J.-Y., Guo, J.-J., & Tang, L.-D. (2019). Prediction of entropy and Gibbs free energy for nitrogen. *Chemical Engineering Science*, *202*(1), 70-74.

Jia, C. S., Zhang, L. H., & Wang, C. W. (2017). Thermodynamic properties for the lithium dimer. *Chemical Physics Letters*, *667*(1), 211–215.

Jiang, R., Jia, C. S., Wang, Y. Q., Peng, X. L., & Zhang, L. H. (2019). Prediction of enthalpy for the gases CO, HCl, and BF. *Chemical Physics Letters*, *715*(1), 186-189.

Khordad, R., Mirhosseini, B., & Mirhosseini, M. M. (2019). Thermodynamic Properties of a GaAs Quantum Dot with an Effective-Parabolic Potential: Theory and Simulation. *Journal of Low Temperature Physics*, *197*(1), 95-110.

Khordad, R., & Sedehi, H. R. (2018). Thermodynamic Properties of a Double Ring-Shaped Quantum Dot at Low and High Temperatures. *Journal of Low Temperature Physics*, *190*(3), 1-13.

Khosla, P., Arora, S., Gupta, Y., Priyanka, & Sharma, R. (2023). Hydrostatic Pressure Efect on the Thermodynamic Properties of Quantum Wire Under a Crossed Electromagnetic Field. *Journal of Low Temperature Physics*.

https://doi.org/https://doi.org/10.1007/s10909-023-02990-2

Levai, G. (1994). Solvable potentials associated with su (1,1) algebras: a systematic study, . *Journal of Physics A: Mathematical and General*, *27*(11), 3809-3828.

Li, B., Liu, W., Zhu, X., Lin, S., Yang, Y., Yang, Q., & Jin, P. (2019). Pressure-dependent photoluminescence of CdSe/ZnS quantum dots: critical point of different pressure regimes. *Phys. Lett. A.*, *383*(1483). https://doi.org/https://doi.org/10.1016/j

Li, H., & Kusnezov, D. (1999). Group theory approach to band structure: Scarf and Lamé Hamiltonians. *Physical Review Letters*, *83*(7), 1283-1287.

Lin, Y. C., Chou, W. C., Susha, A. S., Kershaw, S. V., & Rogach, A. L. (2013). Photoluminescence and time-resolved carrier dynamics in thiol-capped CdTe nanocrystals under high pressure. *Nanoscale 5*(3400). https://doi.org/https://doi.org/10.1039/C3NR33928A

Mano, T., Kuroda, T., Sanguinetti, S., Ochiai, T., Tateno, T., Kim, J., Noda, T., Kawabe, M., Sakoda, K., Kido, G., & Koguchi, N. (2005). Self-assembly of concentric quantum double rings. *Nano Letters*, *5*(3), 425-428.

Morse, P. M. (1929). Diatomic molecules according to the wave mechanics. II. Vibrational levels. *Physical Review Letters*, *34*(1), 57-64.

Nikiforov, A. F., & Uvarov, V. B. (1988). *Special Functions of Mathematical Physics*. Springer.

Okon, I., & al., e. (2022). Approximate Solutions, Thermal Properties, and Superstatistics Solutions to Schrödinger Equation. *Advances in High Energy Physics*, *2022*, 1-18.

Okon, I. B., Popoola, O., & Isonguyo, C. N. (2017). Approximate Solutions of Schrodinger Equation with Some Diatomic Molecular Interactions Using Nikiforov-Uvarov Method. *Advances in High Energy Physics*, *2017*, 1-25.

Okorie, U. S., Edet, C. O., Ikot, A. N., Rampho, G. J., & Sever, R. (2020). Thermodynamic functions for diatomic molecules with modified Kratzer plus screened Coulomb potential. *Indian Journal of Physics*, *95*(3), 411-421.

Okorie, U. S., & Ibekwe, E. E. (2018). Thermodynamic Properties of the Modified Yukawa Potential. *Journal of the Korean Physical Society*, *73*(9), 1211-1218.

Okorie, U. S., Ikot, A. N., Chukwuocha, E. O., & Rampho, G. J. (2020). Thermodynamic properties of improved deformed exponential-type potential (IDEP) for some diatomic molecules. *Results in Physics*, *17*, 1-7.

Omar Mustafa, Z. A. (2020). PDM-charged particles in PD-magnetic plus Aharonov–Bohm flux fields: Unconfined “almost-quasi-free” and confined in a Yukawa plus Kratzer exact solvability. *Chinese Journal of Physics*, *65*, 554-566.

Onate, C. A., Okoro, J. O., Adebimpe, O., & Lukman, A. F. (2018). Eigen solutions of the Schrödinger equation and the thermodynamic stability of the black hole temperature. *Results in Physics*, *10*(1), 406-410.

Orabi, E. A., & Faraldo-Gómez, J. D. (2020). New Molecular-Mechanics Model for Simulations of Hydrogen Fluoride in Chemistry and Biology. *J Chem Theory Comput.*, *16*(8), 5105-5126.

Ortega, G. V., & Hernandez, L. A. (2018). Thermodynamic properties of diatomic molecule systems under SO

(2, 1)-anharmonic Eckart potential. *International Journal of Quantum Chemistry*, *118*(14).

Pareek, A., Dom, R., Gupta, J., Chandran, J., Vivek Adepu, & Borse, P. H. (2020). Insights into renewable hydrogen energy: Recent advances and prospects. *Materials Science for Energy Technologies*, *3*, 319-327.

Pekeris, C. L. (1934). The rotation-vibration coupling in diatomic molecules. *Physical Review*, *45*(2), 98-103.

Peleshchak, R. M., Kuzyk, O. V., & Dan'kiv, O. O. (2020). The influence of the electrically inactive impurity on the energy spectrum of electron and hole in InAs/GaAs heterostructure with InAs quantum dots. *Rom. J. Phys.*, *65*(610).

Rosen, N., & Morse, P. M. (1932). On the Vibrations of Polyatomic Molecules. *Physical Review*, *42*(1), 210-217.

Sedehi, H. R., & Khordad, R. (2021). Magnetocaloric effect, magnetic susceptibility and specific heat of tuned quantum dot/ring systems. *Physica E: Low-dimensional Systems and Nanostructures,*, *134*, 1-6.

Solaimani, M. (2021). Effects of geometry and electric and magnetic fields on the thermal properties of two-dimensional semiconducting nanoporous superlattices. *Journal of Physics and Chemistry*, *149*, 1-7.

Soopy, K. K., Li, Z., Tang, T., Sun, J., Xu, B., Zhao, C., & Najar, A. (2021). In (Ga) N Nanostructures and Devices Grown by Molecular Beam Epitaxy and Metal-Assisted Photochemical Etching. *Nanomaterials*, *11*(126), 1-28.

Sukumar, C. V. (1985). Supersymmetric quantum mechanics of one-dimensional systems. *Journal of Physics A: Mathematical and General*, *18*(15).

Suparmi, A., & Cari, C. (2014). Bound State Solution of Dirac Equation for Generalized Pöschl-Teller plus Trigomometric Pöschl-Teller Non-Central Potential Using SUSY Quantum Mechanics. *Journal of Mathematical and Fundamental Sciences*, *46*(3).

Suparmi, A., Cari, C., & Faniandari, S. (2020). Eigen solutions of the Schrodinger equation with variable mass under the influence of the linear combination of modified Woods–Saxon and Eckart potentials in toroidal coordinate. *MOLECULAR PHYSICS 118*(24). https://doi.org/10.1080/00268976.2020.1781946

Vicente, A. G. J., Castro, L. B., & Obispo, A. E. (2021). Remarks on Thermodynamic Properties of a Double Ring-Shaped Quantum Dot at Low and High Temperatures. *Journal of Low Temperature Physics*, *202*(3), 372-381.

Wang, N., Cai, Y., & Zhang, R. Q. (2008). Growth of nanowires. *Materials Science and Engineering: R: Reports*, *60*(1-6), 1-51. https://doi.org/https://doi.org/10.1016/j.mser.2008.01.001

Warburg, E. (1881). Magnetische untersuchungen. *Annalen der Physik*, *249*(5), 141-164.

Witten, E. (1981). Dynamical breaking of Supersymmetry. *Nuclear Physics B*, *188*(3), 513-554.

Xiao, Z., Kang, Z., A., A., Bansihev, Breidenich, J., Scripka, D. A., Christensen, J. M., Summers, C. J., Dlott, D. D., Thadhani, N. N., & Zhou, M. (2016). Laser-excited optical emission response of CdTe quantum dot/polymer nanocomposite under shock compres-sion. *Appl. Phys. Lett.* , *108*. https://doi.org/https://doi.org/10.1063/1.4939701

Yin, C., Cao, Z., & Shen, Q. (2010). Why SWKB approximation is exact for all

SIPs. *Annals of Physics, 325*, 528-534.

Zeiri, N., Naifar, A., Abdi-Ben Nasrallah, S., & Said, M. (2019). Third nonlinear optical susceptibility of CdS/ZnS core-shell spherical quantum dots for optoelectronic devices. *Optik, 176*(2019), 162-167.

Zhang, Y., Hou, L., Ren, Z., Li, X., & Wilde, G. (2016). Magnetic properties and magnetocaloric effect in TmZnAl and TmAgAl compounds. *Journal of Alloys and Compounds, 656*(1), 635-639.

Zhang, Y. e. a. (2016). Study of the magnetic phase transitions and magnetocaloric effect in Dy2Cu2In compound. *Journal of Alloys and Compounds, 667*(1), 130-133.